2019

Arrival management for eVTOL aircraft in on-demand urban air mobility

Priyank Pradeep
Iowa State University

Arrival management for eVTOL aircraft in on-demand urban air mobility

by

Priyank Pradeep

A dissertation submitted to the graduate faculty

in partial fulfillment of the requirements for the degree of

DOCTOR OF PHILOSOPHY

Major: Aerospace Engineering

Program of Study Committee:
Peng Wei, Major Professor
A Ram (Bella) Kim
Benjamin Ahn
Leifur Thor Leifsson
Lizhi Wang

The student author, whose presentation of the scholarship herein was approved by the program of study committee, is solely responsible for the content of this dissertation. The Graduate College will ensure this dissertation is globally accessible and will not permit alterations after a degree is conferred.

Iowa State University

Ames, Iowa

2019

DEDICATION

To the Almighty God, Guru, Family and Advisor!

TABLE OF CONTENTS

Page

LIST OF TABLES

LIST OF FIGURES

ACKNOWLEDGEMENTS

I want to take this opportunity to express my thanks to those who helped me with various aspects of Ph.D. program at Iowa State University.

First and foremost, Dr. Peng Wei for his guidance, patience, and support throughout this research. His insights and words of encouragement have often inspired me and renewed my hopes for completing my graduate education. I will forever be grateful for the knowledge and skills that I have gained working in his group. His leadership style of empowerment and trust has been a very positive impact on my research productivity and morale throughout the program.

Second, I would also like to thank my committee members for their efforts and contributions to this work: Dr. A Ram (Bella) Kim, Dr. Benjamin Ahn, Dr. Leifur Thor Leifsson and Dr. Lizhi Wang.

Third, my sincere gratitude towards Dr. Hok K Ng, Dr. Gilbert Wu, Dr. Chetan Kulkarni, Mr. Christopher Teubert, Dr. Matteo Corbetta and Dr. Indranil Roychoudhury from NASA Ames Research Center for providing valuable help and guidance on my research and making my visit at NASA Ames memorable.

Fourth, I am thankful to Dr. Sang Gyun Park and Dr. Kshitij Mall for helping me out with GPOPS-II/IPOPT optimal control solver.

Fifth, my dear labmates (Abdullah, Anwar, Guodong, Imke, Josh, Marc, Xufang and Xuxi) for making my Ph.D. journey memorable and filled with fun.

Last but not least, my parents (Pradeep and Vasanthi), wife (Prathipa), sister (Trishna) and my in-laws (Pandiyan and Vennila) for their encouragement and support to complete this program. Also, my in debt gratitude for my parents (Pradeep and Vasanthi) and my late grandmother (Sulochana) who unconditionally supported me in all my endeavors.

ABSTRACT

The electric vertical takeoff and landing (eVTOL) aircraft can alleviate transportation congestion on the ground by utilizing three-dimensional airspace efficiently. However, the endurance (specific energy) of Lithium-ion Polymer (Li-Po) batteries imposes severe constraints on the operational time-span of an eVTOL on urban air mobility (UAM) passenger transportation mission.

The first part of the research focuses on the generation of energy efficient trajectories for eVTOLs with the assigned required times of arrival (RTA)s. The problem formulations are performed in multiphase optimal control framework with energy as the performance index for the following eVTOL aircraft types: (i) multirotor and (ii) tandem tilt-wing. These two types of eVTOLs are chosen because of their performance characteristics falling at the two extremes of the performance spectrum of eVTOLs. The proposed multiphase optimal control problem formulations and the corresponding numerical solutions enable an eVTOL to meet the assigned RTA and achieve the most energy efficient arrival trajectory, which is a critical enabler for the safe and efficient future eVTOL operations for passenger transportation and cargo delivery in UAM environment. The problem formulations are applied to a UAM passenger transport use cases with (i) EHang 184, (ii) Airbus Vahana, and (iii) the Uber Elevate proposed vertiport concept in numerical simulations.

The second part of the research involves arrival sequencing and scheduling problem formulation in UAM context for a mixed fleet (winged/wingless) of eVTOLs expected to land on a vertiport. Based on anticipated UAM traffic density in emergent (low) and early expanded (moderate/high) operations, two separate vertiport arrival procedures have been proposed for the problem. The arrival procedure for early expanded operations is proposed based on arrival procedure of emergent operations as a baseline with the addition of metering gate(s) on the boundary of the terminal area (a circular area of radius 400 m around a vertiport) and multiple landing pads on the vertiport. The objective of the problem is to minimize the makespan (landing completion time) of a given

set of eVTOLs, which is equivalent to maximizing the vertiport arrival throughput. A heuristic approach called insertion, and local search (ILS) [Malik and Jung (2016)] combined with two different scheduling methods: i) mixed-integer linear programming (MILP) and ii) time-advance (TA) are proposed to optimize the landing order (sequence) and makespan of the mixed fleet of eVTOLs. Next, the impact of the number of landing pads (N) on the vertiport arrival throughput is studied to aid in early expanded UAM operations (moderate/high traffic density). Finally, sensitivity analysis is performed to see the impact of the following on the sequencing and scheduling algorithms: i) the number of eVTOLs expected to land (n) and ii) the number of eVTOLs used in the local neighborhood search (k). Through numerical simulations and sensitivity analysis, our algorithms demonstrated real-time scheduling capabilities for on-demand UAM arrival operations, which can be used as a potential future service for UAM vertiports and terminal airspace.

Keywords: Electric Vertical Takeoff and Landing (eVTOL), Multiphase Optimal Control, Trajectory Optimization, Large-Scale Mixed Integer Linear Programming (MILP) and Urban Air Mobility (UAM).

CHAPTER 1. OVERVIEW

1.1 Introduction

Every day, millions of person-hours are spent unproductively in cities across the world due to road-traffic congestion. In 2014, the congestion caused 3.1 billion gallons of extra fuel burn in the US alone. Transportation as a whole accounted for approximately 33 % of CO_2 emissions in the US, of which 80 % were from cars and trucks traveling on the roadway system [Schrank et al. (2015)]. Commuting time has an adverse impact on physical activity and cardio-respiratory fitness (CRF) of human beings [Hoehner et al. (2012)]. A study in the American Journal of Preventative Medicine, for example, found that those who commute more than 10 miles were at increased odds of elevated blood pressure [Hoehner et al. (2012)].

The eVTOL aircraft can alleviate transportation congestion on the ground by utilizing three-dimensional airspace efficiently, just as skyscrapers allowed cities to use limited land more efficiently. The envisioned concept of urban air mobility (UAM) involves a network of small, electric aircraft that take off and land vertically (eVTOL), and, can enable rapid and reliable transportation between suburbs and cities and, ultimately, within cities [Uber-Elevate (2016); Consulting (2018); Airbus-A^3 (2018)].

Recently, technological advances have made it possible to build and flight test eVTOL aircraft [Uber-Elevate (2016); Airbus-A^3 (2018); Thipphavong et al. (2018)]. Over a dozen companies, for example, Airbus A^3, Aurora Flight Sciences, EHang, Jobby Aviation, Kitty Hawk, Leonardo, Lilium, Terrafugia, Volocopter, etc., with many different design approaches, are passionately working to make eVTOLs a reality. Despite various designs, they all have distributed electric propulsion (DEP) system in common. Considerable power-to-weight, efficiency, reliability and operational flexibility improvements are possible utilizing DEP technology in eVTOLs compared to the rotor system of conventional helicopters [Uber-Elevate (2016); Airbus-A^3 (2018); Snyder (2017); Kim

et al. (2018); Thipphavong et al. (2018)]. The conventional helicopters are capable of VTOL, but the noise generated by them has been significant enough to compel communities to take legal action on their usage in UAM [Thipphavong et al. (2018)]. DEP powered eVTOLs have a higher downwash velocity compared to conventional helicopters that permits a more rapid vertical descent without entering a vortex ring state [Uber-Elevate (2016)]. Engine failure accounts for 18 % of general aviation accidents when combined with fuel management errors. The use of DEP, controllers, and a redundant battery bus architecture avoids the problems of catastrophic engine failure by having full propulsion system redundancy [Uber-Elevate (2016); Airbus-A^3 (2018); Snyder (2017)]. The eVTOLs also have an advantage of zero operational emissions as they use electric propulsion [Uber-Elevate (2016); Prevot et al. (2016); Airbus-A^3 (2018)]. However, low specific energy of Lithium-ion Polymer (Li-Po) batteries imposes critical constraints on the operational time span of an eVTOL aircraft on UAM passenger transportation mission [Uber-Elevate (2016)].

1.2 Background and Literature Review

The commercial UAM operations have occurred in the United States since the 1940s in Los Angeles (LA) and New York City (NYC) using helicopters to transport people and mail between dozens of locations, but they ceased from LA and NYC in 1968 and 1977 respectively because of multiple tragic incidents [Thipphavong et al. (2018)]. However, current aviation technologies have reached a level of maturity to enable UAM using quiet and efficient manned and unmanned vehicles to conduct on-demand and scheduled operations [Uber-Elevate (2016); Airbus-A^3 (2018); Thipphavong et al. (2018)]. At present, there is an increase in consumer demand in many cities worldwide towards developing an air taxi service in UAM environment [Uber-Elevate (2016); Thipphavong et al. (2018)]. Market research on UAM has shown that in the US alone, airport shuttle and air taxi markets have a market value of $ 500 billion at the market entry price points in the best-case unconstrained scenario [Hamilton (2018)].

Since 2013, NASA [Prevot et al. (2016)] and its collaborators from government, industry, and academia have contributed to the research and development of UAS traffic management (UTM). They have been focused on small UAS operations, which include cargo delivery proposed by Amazon and Google. However, from 2016 onwards the possibility of urban air mobility (UAM) has also been explored by NASA and university researchers. NASA and its key partners envision development of UAM concept of operations (CONOPs) in the following three stages [Thipphavong et al. (2018)]:

(i) Emergent UAM operations involving low air-traffic density with a small set of fixed routes between a few vertiports.

(ii) Early expanded UAM operations involving higher air-traffic density flights in a small network of vertiports to feed a common hub.

(iii) Mature UAM operations involving high air-traffic density flights in a network with multiple hubs and orders-of-magnitude more eVTOLs.

Significant work has been performed towards defining high-level descriptions of both emergent and early expanded operational concepts for UAM [Prevot et al. (2016); Uber-Elevate (2016); Airbus-A^3 (2018); Altawy and Youssef (2016); Thipphavong et al. (2018); Mueller et al. (2017); Bosson and Lauderdale (2018)]. The investment of resources for UAM research and development includes the following: i) researchers and builders of takeoff and landing areas (TOLA)s, gates, staging stands and taxiway i.e. vertiport infrastructure [Vascik and Hansman (2019)]; ii) researchers of the airspace integration concepts, technologies, and procedures; and iii) eVTOL manufacturers; to conduct UAM operations safely and efficiently in the near future [Thipphavong et al. (2018); Bosson and Lauderdale (2018); Vascik and Hansman (2019)].

Most of the UTM and UAM operations of eVTOLs are expected to be under limited battery endurance and vertiport capacity during emergent and early expanded UAM operations [Thipphavong et al. (2018)]. Also, to realize mature UAM operations dream, orders-of-magnitude more aircraft than that operate today in the current airspace would be required to serve the urban public in the metropolitan areas [Mueller et al. (2017)].

Before the large-scale fully autonomous UAM operations become true, the first bottle-neck of UAM traffic throughput is expected to appear at the vertiport (or skyport) terminal airspace [Uber-Elevate (2016); Mueller et al. (2017); Thipphavong et al. (2018); Vascik and Hansman (2019)]. In UAM operations, we anticipate that the arrival phase (compared with departure) will be one of the most safety-critical phases of flight.

In air transportation world, for safe and efficient arrivals, researchers have worked on the following: i) generation of fuel-efficient (minimum fuel), time-efficient (minimum time) and noise-abatement arrival trajectories of commercial jetliners [Park and Clarke (2012); Robinson III and Kamgarpour (2010); Clarke et al. (2004); Pradeep and Wei (2017); Jin et al. (2013); Cao et al. (2013); Dalmau et al. (2016); Coppenbarger et al. (2009); Xu and Prats (2017)]; and ii) arrival sequencing and scheduling algorithms/tools for maximizing the throughput for minimizing the delay of commercial air-traffic [Dear (1976); Malik and Jung (2016); Neuman and Erzberger (1991); Balakrishnan and Chandran (2010); Anagnostakis et al. (2001); Hu and Chen (2005)].

However, little research [Pradeep and Wei (2018a,b); Kleinbekman et al. (2018); Bosson and Lauderdale (2018)] in UAM has been carried out on the trajectory optimization and arrival sequencing and scheduling of eVTOLs.

1.3 Motivation

The motivation for this research comes from the fact that for passenger transportation and cargo delivery by eVTOLs to be successful many critical operational challenges must be overcome [Vascik and Hansman (2019); Thipphavong et al. (2018); Bosson and Lauderdale (2018); Uber-Elevate (2016); Mueller et al. (2017)].

1.3.1 Generate Energy Efficient Trajectory with RTA constraint

Studies and operational trials have been undertaken to investigate the performance and behavior of the assigned RTA for the fixed-wing aircraft [Wing (2005); Prevot et al. (2003); Coppenbarger et al. (2004)]. The assigned RTA (control mechanism) enables aircraft to meet a controlled time

of arrival (CTA) imposed by Air Traffic Control (ATC) at the meter fix [Smedt et al. (2013)]. The assigned RTA to the meter fix can be met either using speed adjustment strategy or path modification strategy or combination of both [Smedt et al. (2013); Nikoleris et al. (2016); Xu and Prats (2017)]. RTA improves air traffic operations by increasing the overall predictability of traffic that is easier to handle (fewer conflicts, information comes well in advance). Since the goals for integration of UAM with existing National Airspace System (NAS) includes imposing minimal additional: (i) workload on air traffic controllers and (ii) requirements or burdens on NAS [Thipphavong et al. (2018)]. Therefore, the precise implementation of 4D trajectory operations in UAM requiring each eVTOL aircraft to precisely follow 4D trajectory consisting of a planned 3D path (spatial) and an along-path time constraint will assure adequate separation between eVTOLs and optimize the use of limited NAS resources.

The energy required to complete a UAM mission by an eVTOL aircraft must be less than the energy available in the onboard Lithium-ion polymer (Li-Po) battery pack. Also, from the certification point of view eVTOL aircraft may require landing with reserve battery charge/usage time (analogous to reserve fuel in the aircraft). Though DEP is the preferred propulsion choice for the VTOL air taxi, the specific energy (the amount of energy per unit weight provided by the battery) of Li-Po batteries today is insufficient for long-range commutes [Uber-Elevate (2016); Thipphavong et al. (2018)]. Therefore, planning and flying minimum energy trajectories is critical to safe and efficient UAM operations.

Therefore, the first part of the research is motivated to generate an energy efficient arrival trajectory with RTA constraint for a given CONOP and an eVTOL aircraft in UAM.

1.3.2 Arrival Sequencing and Scheduling of eVTOLs

Before the large-scale fully autonomous matured UAM operations [Thipphavong et al. (2018)]) become true, the first bottleneck of UAM traffic throughput is expected to appear at the vertiport (or skyport) terminal airspace. In UAM operations, we anticipate that the arrival phase (compared with departure) will be one of the most safety-critical phases of flight. This is because of the follow-

ing reasons: (1) arrival traffic will be restricted by the capacity of vertiports, and air traffic is, in general, dynamic and complex in terminal airspace; (2) flight endurance of eVTOL aircraft will be limited by the specific energy (the amount of energy per unit weight provided by the battery) and state-of-charge (SOC) of lithium-ion polymer (Li-Po) batteries [Uber-Elevate (2016); Pradeep and Wei (2018a,b)]. Therefore, UAM operations will require safe and efficient services similar to ATC services in National Airspace System (NAS) for commercial aircraft [Uber-Elevate (2016); Mueller et al. (2017)]. However, matured UAM operations will require introducing orders-of-magnitude more eVTOL aircraft in given airspace then that can be accommodated by the current air traffic control (ATC) system [Mueller et al. (2017)].

Our research on solving the arrival sequencing and scheduling for eVTOL aircraft in UAM is inspired by deterministic modeling of arrival sequencing and scheduling problem in the terminal area for commercial air traffic [Hong et al. (2018); Pawelek et al. (2017); Neuman and Erzberger (1990); Erzberger and Itoh (2014); Anagnostakis et al. (2001); Malik and Jung (2016); Balakrishnan and Chandran (2006)]. First-come-first-served (FCFS), is the most straightforward arrival sequencing and scheduling method as it schedules the aircraft in the order of their estimated time of arrival (ETA) to the metering points (gates and runway threshold) [Neuman and Erzberger (1990)]. The FCFS sequencing order provides a sense of fairness and is easy to implement for the ATC. However, it can not achieve optimal throughput in UAM because of very different nominal cruise speeds of various eVTOL aircraft. Therefore, mixed fleet of eVTOLs (winged/wingless), vertiport capacity and the low specific energy of Li-Po batteries provides an incentive to deviate from the FCFS order and find the most efficient sequence (landing order) with optimal spacing between the eVTOL aircraft to maximize vertiport throughput for UAM arrival operations.

Finding an optimal arrival sequencing order is a non-deterministic polynomial time (NP) hard problem [Malik and Jung (2016); Balakrishnan and Chandran (2006); Zhan et al. (2010); Hu and Chen (2005); Psaraftis (1980)]. Hence, instead of finding an exact solution for sequencing order, many researchers have investigated heuristic and meta-heuristic optimization algorithms for commercial air traffic [Malik and Jung (2016); Balakrishnan and Chandran (2006); Zhan et al. (2010);

Hu and Chen (2005); Psaraftis (1980)]. Furthermore, due to the anticipated dynamic environment of on-demand UAM operations, it might not be possible to compute the optimal arrival sequence of eVTOLs that deviates significantly from the FCFS order in real time. However, we anticipate that arrival sequencing and scheduling service provider for UAM will have the computing capability to explore other sequences by shifting eVTOL landing slots by a small number from its FCFS order like the commercial aircraft in the terminal area [Malik and Jung (2016); Balakrishnan and Chandran (2006); Hu and Chen (2005); Dear (1976)]. This dissertation aims to solve eVTOL arrival sequencing and scheduling problem in UAM using insertion and local search (ILS) heuristic approach [Malik and Jung (2016)].

In commercial air traffic world, one possible approach to decrease the average delay incurred by aircraft and maximize the runway throughput is to accelerate from their ideal speeds. This strategy is known as time advance (TA) [Neuman and Erzberger (1990); Balakrishnan and Chandran (2006)]. Similarly, to maximize the throughput at a vertiport, given the anticipated randomness in on-demand traffic in UAM and different cruise speeds of various eVTOLs, time-advance (TA) strategy [Neuman and Erzberger (1990); Balakrishnan and Chandran (2006)] has been combined with the a heuristic method in this dissertation.

1.4 Research Objectives

The research objectives of this dissertation are to address the following critical operational challenges in UAM for passenger transportation and cargo delivery by eVTOLs:

- Generate the most energy efficient arrival trajectory given limited battery endurance, specified CONOP, and eVTOL type.
- Meet the assigned RTA constraint given the safe eVTOL aircraft separation requirement and limited vertiport arrival time slots.
- Formulate and solve the arrival sequencing and scheduling problem for a mixed fleet (winged/wingless) of eVTOLs to enable safe and efficient UAM operations.

1.5 Research Contributions

The contribution of this dissertation are as follows:

- One of the first researchers to study arrival management of eVTOL aircraft in on-demand UAM and initiator for European UAM research in collaboration with TU Delft.
- Formulated multiphase optimal control problem for winged and wingless eVTOL aircraft for performing energy efficient arrival in UAM.
- Researched and developed in-house algorithms to solve arrival sequencing and scheduling problem for safe and efficient UAM arrival operations. These algorithms can be potentially used by arrival sequencing and scheduling service providers in UAM operations.
- Performed extensive simulations to aid policymakers in decision making for designing arrival procedures in UAM environment.

1.6 Organization of the Dissertation

The rest of the dissertation is organized as follows: In chapter 2 of the dissertation, we present multiphase optimal control framework for a multirotor eVTOL aircraft (like CityAirbus, EHang 184 and Volocopter 2X) [EHang-184 (2018); CityAirbus (2017); Volocopter (2018)] to perform energy efficient arrival with required time of arrival (RTA) constraint for a given concept of operation (CONOP). The problem formulation is applied to a UAM passenger transportation use case with EHang 184 eVTOL aircraft, and an Uber proposed vertiport for five different types of CONOPs. Finally, the energy consumed for all the CONOPs is compared to propose the most energy efficient CONOP for a multirotor eVTOL on UAM passenger transportation mission. In chapter 3, we focus on the formulation of a fixed final time multiphase optimal control problem with energy consumption as the performance index for a tandem tilt-wing eVTOL aircraft and Airbus Vahana proposed CONOP. The proposed multiphase optimal control problem formulation and the numerical solution enable the eVTOL aircraft to meet the assigned required time of arrival (RTA) with the

optimal speed profile for the most energy efficient arrival for Airbus Vahana CONOP. The problem formulation is applied to a UAM passenger transport use case with Airbus Vahana eVTOL aircraft, and the Uber Elevate proposed vertiport concept in numerical simulations. In chapter 4, we present validation of the multiphase optimal control model using a commercial quadrotor DJI Phantom 4.0. We have used DJI Phantom 4.0 for the validation because of its known performance characteristics to the remote pilots and public. In chapter 5, we formulate and solve arrival sequencing and scheduling problem for a mixed fleet of eVTOLs (winged/wingless) expected to land on a vertiport. Based on anticipated UAM traffic density in emergent (low) and early expanded (moderate/high) operations [Vascik and Hansman (2019); Bosson and Lauderdale (2018); Thipphavong et al. (2018)], two separate vertiport arrival procedures have been proposed for the problem. A heuristic approach called insertion, and local search (ILS) [Malik and Jung (2016)] combined with two different scheduling methods: i) mixed-integer linear programming (MILP) and ii) time-advance (TA) is proposed to optimize the landing order (sequence) and makespan of the mixed fleet of eVTOLs. Finally, sensitivity is performed to understand the impact of various factors on the performance of the proposed algorithm. Chapter 6 summarizes the work of this dissertation and discusses future directions.

CHAPTER 2. ENERGY EFFICIENT ARRIVAL OF MULTIROTOR EVTOL

2.1 Introduction

In this chapter, multiphase optimal control framework for a multirotor eVTOL aircraft (like CityAirbus, EHang 184 and Volocopter 2X) [EHang-184 (2018); CityAirbus (2017); Volocopter (2018)] to perform energy efficient arrival with required time of arrival (RTA) constraint for a given concept of operation (CONOP) is presented.

2.2 Multiphase Optimal Problem Formulation

2.2.1 eVTOL Aircraft Model

In this chapter of the dissertation, the multirotor eVTOL aircraft is modeled based on specifications of EHang 184 EHang-184 (2018). However, the multiphase optimal control [Kirk (2012); Bryson (2018)] problem formulation presented in this dissertation can be easily modified and used for other multirotor eVTOL models such as CityAirbus CityAirbus (2017) and Volocopter 2X Volocopter (2018).

EHang 184 has four arms with each arm consisting of two identical coaxial counter-rotating rotors (X8-configuration) as shown in Figure 2.1.

2.2.2 Trajectory Optimization

The lateral path between the initial position of the eVTOL in-air (cruise phase) and the vertiport is assumed to be a geodesic path. Therefore, only the vertical trajectory of the eVTOL aircraft is free for optimization. However, since constraint has been imposed on the arrival time of eVTOL aircraft, the problem involves generation of an energy-optimal vertical path for the eVTOL aircraft with fixed final time. In this dissertation, the vertical trajectory optimization is formulated as a

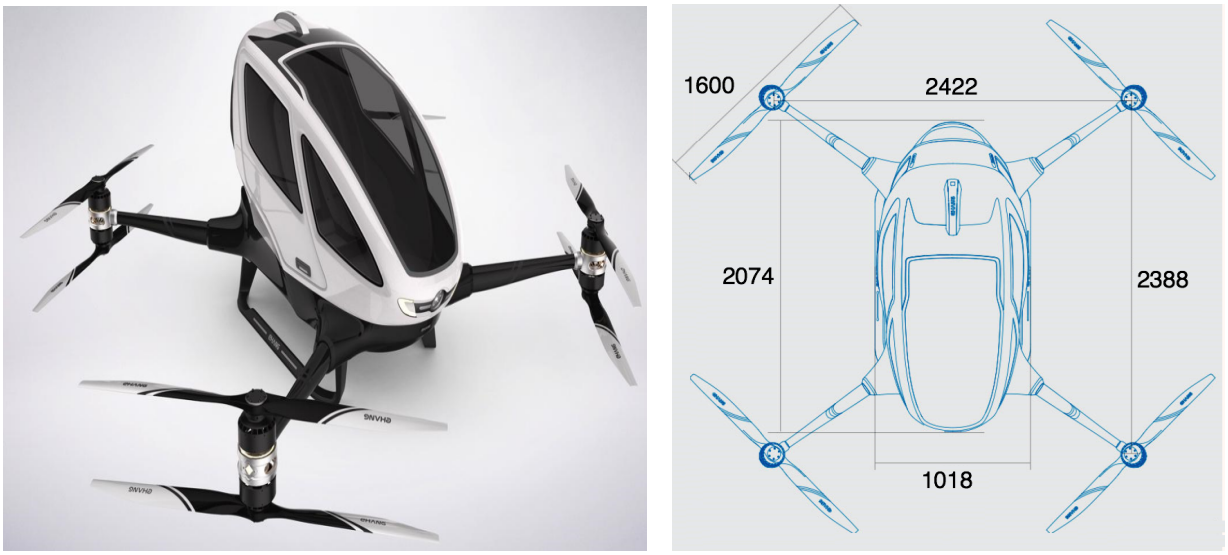

Figure 2.1: EHang 184: Coaxial Multirotor eVTOL Aircraft with X8-Configuration [EHang-184 (2018)]

multiple phase optimal control problem of Lagrange type as follows [Park and Clarke (2012); Rao et al. (2010)]:

$$J = \sum_{N=1}^{2} \int_{t_0^N}^{t_f^N} L^N(y(t), u(t), t)dt \tag{2.1}$$

subject to the first-order dynamic constraints:

$$\frac{dy(t)}{dt} = f^N(y(t), u(t), t) \tag{2.2}$$

subject to the path constraints:

$$C_{min}^N \leq C^N(y(t), u(t), t) \leq C_{max}^N \tag{2.3}$$

subject to the control bounds:

$$u_{min}^N \leq u(t) \leq u_{max}^N \tag{2.4}$$

where L is the Lagrangian cost function, N is the vertical flight phase (N = 1 for cruise and N = 2 for descent), y(t) is the state vector, u(t) is the control vector and C(y(t), u(t), t) represents the path constraints.

2.2.3 Flight Dynamics Model

In quadrotors roll, pitch and yaw angles are controlled by using various differential thrust mechanism across the rotors. For example, differential thrust between opposite motors provides roll and pitch moments [Hoffmann et al. (2007)]. Previously, researchers [Bottasso et al. (2005); Yomchinda et al. (2011); Johnson (1977)] have successfully decoupled longitudinal and lateral dynamics for helicopters with the conventional design. In general, quadrotors have a more symmetrical design (the location of rotors and the axis of rotation w.r.t center of gravity) than the conventional helicopters. Hence, to simplify the optimal control problem and reduce the computational time, the longitudinal dynamics of the multirotor eVTOL aircraft has been decoupled from lateral dynamics [Bottasso et al. (2005); Yomchinda et al. (2011); Johnson (1977)]. This allows us to solve the vertical trajectory generation problem as 2D flight dynamics problem in the vertical plane.

The two-dimensional longitudinal dynamics model of the aircraft in a fixed inertial frame of reference is as follows (shown in Figure 2.2):

$$\frac{dV_x}{dt} = \frac{T\sin\theta - D\cos\gamma}{m} \tag{2.5}$$

$$\frac{dV_h}{dt} = \frac{T\cos\theta - D\sin\gamma - mg}{m} \tag{2.6}$$

$$\frac{dx}{dt} = V_x \tag{2.7}$$

$$\frac{dh}{dt} = V_h \tag{2.8}$$

$$T = \sum_{i=1}^{4} (T_{arm})_i \tag{2.9}$$

where [x,h] is the position vector (along track distance, altitude) of the center of mass relative to the origin (inertial frame of reference), θ is the rotor tip-path-plane pitch angle, T is the net thrust, D is the net drag, $(T_{arm})_i$ is the net thrust produced by the i^{th} arm (two counter-rotating coaxial rotors), m is the mass, [V_x,V_h] are the horizontal and vertical components of the true airspeed and g is the acceleration due to gravity. Therefore, the state vector and control vector are defined as:

$$y(t) = [x, h, V_x, V_h]^T \tag{2.10}$$

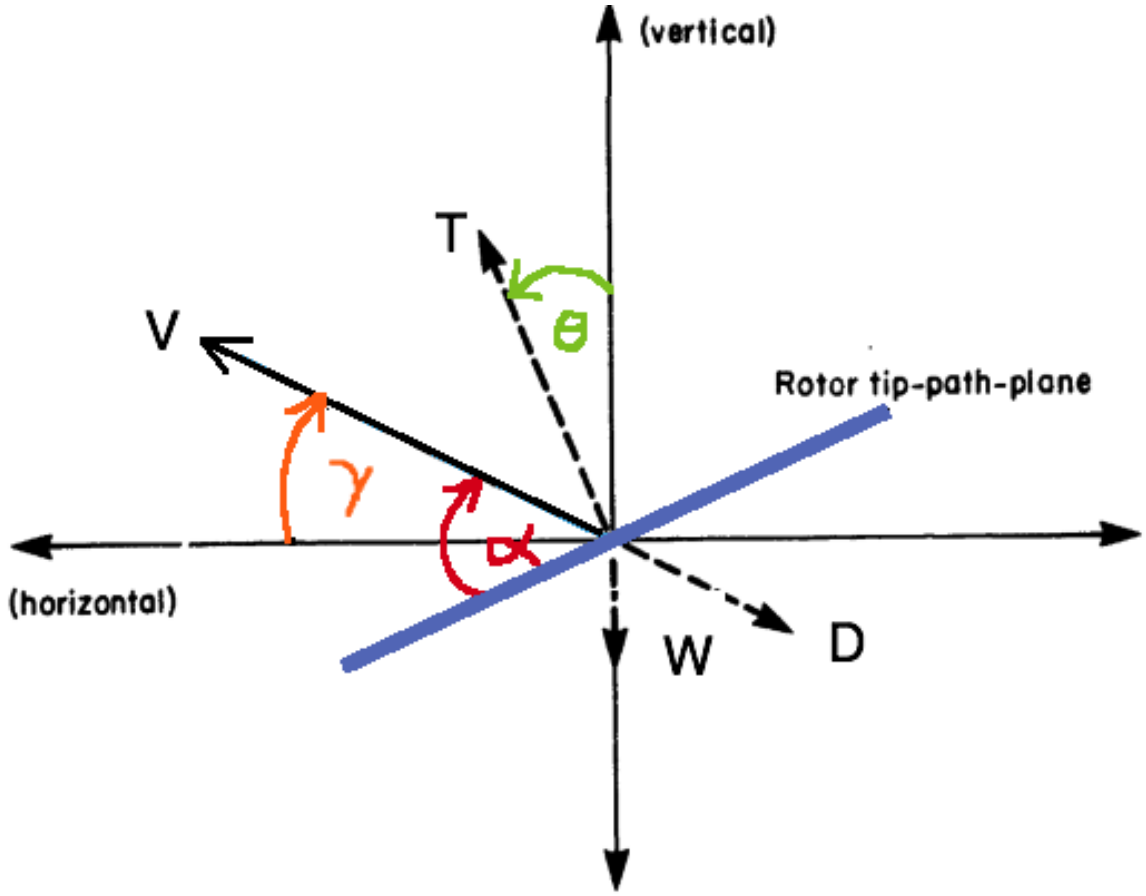

Figure 2.2: Definition of the Aircraft's Position, Velocity and Forces

$$u(t) = [\theta, T]^T \tag{2.11}$$

Also, the rotor tip-path-plane pitch angle (θ), the rotor angle of attack (α) and the eVTOL aircraft's flight path angle (γ) are related as following:

$$\alpha = \theta + \gamma \tag{2.12}$$

2.2.4 Drag Model

Based on the maximum ground speed of the aircraft (100 km/hr), the aircraft operates in M $<$ 0.3 flow regime and hence the drag force on the fuselage of the eVTOL aircraft can be modeled

based on the incompressible flow theory. The net drag on the aircraft is assumed to be equivalent to the drag on the fuselage of the aircraft. Therefore, the net drag on the aircraft is calculated as follows [Yomchinda et al. (2011); DeMoss (2007)]:

$$D = \frac{\rho V^2 C_D F}{2} \tag{2.13}$$

where F is the equivalent flat plate area of the fuselage and $C_D = 1$ [Yomchinda et al. (2011)].

The horizontal and vertical components of the drag in fixed inertial frame of reference are as follows:

$$D_x = \frac{\rho V_x^2 C_D F_x}{2} \tag{2.14}$$

$$D_h = \frac{\rho V_h^2 C_D F_h}{2} \tag{2.15}$$

where F_x and F_h are the equivalent front and top flat plate area of the fuselage respectively.

The performance data of EHang 184 used for aerodynamics and momentum theory related computations are as shown in Table 2.1:

Table 2.1: Performance Data of EHang 184

Variable	**Value**
Rotor Diameter (m)	1.6
Mass (kg)	240
Equivalent Front Plate Area (m^2)	2.11
Equivalent Top Plate Area (m^2)	1.47

2.2.5 Momentum Theory in Hover

Using momentum theory [Hoffmann et al. (2007); Heyson (1975); Johnson (2012)], the induced velocity (v_h) in hover is given by:

$$v_h = \sqrt{\frac{T_{rotor}}{2\rho A}} \tag{2.16}$$

where T_{rotor} is the thrust produced by the rotor, A is the rotor disk area (πR^2), R is the radius of the rotor and ρ is the density of the air.

2.2.6 Momentum Theory in Forward Flight

Consider a rotorcraft in forward motion at true airspeed V, with angle of attack α between the air-stream and the rotor disk (tip path plane). The solution for induced velocity (v_i) is [Hoffmann et al. (2007); Heyson (1975); Johnson (2012)]:

$$v_i = \frac{v_h^2}{\sqrt{(V\cos\alpha)^2 + (V\sin\alpha + v_i)^2}} \tag{2.17}$$

In forward flight, the thrust produced by an ideal isolated rotor per power input is given by [Hoffmann et al. (2007); Heyson (1975); Johnson (2012)]:

$$T_{rotor} = \frac{P_{rotor}}{V\sin\alpha + v_i} \tag{2.18}$$

The induced power loss of an isolated rotor ($P_{induced\ rotor}$) in forward flight is given by [Hoffmann et al. (2007); Heyson (1975); Johnson (2012)]:

$$P_{induced\ rotor} = T_{rotor} v_i \tag{2.19}$$

2.2.7 Coaxial Rotor Interference in Forward Flight

The eVTOL aircraft under consideration has 4 arms, with each arm consisting of two identical counter-rotating rotors. Assuming equal thrust produced by the lower and upper rotors of the coaxial rotor system, the net thrust produced by the arm (T_{arm}) is given by:

$$T_{arm} = T_{lower} + T_{upper} = 2T_{rotor} \tag{2.20}$$

Wing theory for a single lifting surface shows that the induced power loss of the arm i.e. coaxial counter-rotating system is [Johnson (2012)]:

$$P_{arm} = 2P_{induced\ rotor}(1 + \chi) \tag{2.21}$$

where χ is the rotor interference factor for the coaxial rotor system. Typically, χ is ≤ 1. However, in the current research the interference factor (χ) for all the rotors is assumed to be 1.0 Johnson (2012).

2.2.8 Power Required by the eVTOL Aircraft

Energy balance equation for a multirotor eVTOL aircraft is given by [Yomchinda et al. (2011); Pradeep et al. (2018)]:

$$\sum_{i=1}^{n} I_i \omega_i \frac{d\omega_i}{dt} = \sum_{i=1}^{n} P_i - P_{required} \tag{2.22}$$

where P_i is the energy supplied to the i^{th} rotor, $P_{required}$ is the instantaneous power required by the aircraft (to overcome induced drag, profile drag, parasite drag and/or gravity to climb), ω_i is the rotational speed of the i^{th} rotor, I_i is the rotational moment of inertia of the i^{th} rotor and n is the total number of rotors on a multirotor eVTOL aircraft. However, based on assumption of quasi-steady flight in the current research, the instantaneous power required in forward flight is equal to the sum of the induced power, parasite power, climb power and profile power [Heyson (1975); Johnson (2012); Leishman (2002)].

$$P_{required} = P_{induced} + P_{parasite} + P_{climb} + P_{profile} \tag{2.23}$$

The profile power exhibits only a slight increase in value with forward speed unless the tip of the rotor is above the critical Mach number [Johnson (2012)]. Since the eVTOL aircraft considered in this research is a low speed aircraft with a small rotor diameter (1.6 m), the profile drag is assumed to be constant in magnitude and hence has a negligible impact on the variation of the instantaneous power required. Therefore, in the current research $P_{required}$ is assumed to be [Johnson (2012)]:

$$P_{required} = P_{induced} + P_{parasite} + P_{climb} \tag{2.24}$$

The induced power loss of the eVTOL aircraft ($P_{induced}$) is equal to the summation of the induced power loss of each arm (P_{arm}). Therefore, the induced power loss of the eVTOL aircraft is given by:

$$P_{induced} = \sum_{i=1}^{4} (P_{arm})_i \tag{2.25}$$

where $(P_{arm})_i$ is the induced power loss of the i^{th} arm as derived in equation 2.21.

The power required to climb and to propel the eVTOL aircraft forward (the parasite power loss) is given by [Johnson (2012)]:

$$P_{parasite} + P_{climb} = TV \sin \alpha \tag{2.26}$$

where T is the net thrust, V is the true airspeed and α is the angle of attack of the tip-path-plane of the rotor.

Therefore, the instantaneous power required ($P_{required}$) in forward flight is given by:

$$P_{required} = \sum_{i=1}^{4} (P_{arm})_i + TV \sin \alpha \tag{2.27}$$

2.2.9 Performance Index of Multiphase Optimal Control

The power supplied by the battery pack to the ideal i^{th} motor at time t is given by Hoffmann et al. (2007):

$$P_i(t) = e_i(t) i_i(t) \tag{2.28}$$

where $e_i(t)$ and $i_i(t)$ is the instantaneous voltage and current across the motor respectively [Hoffmann et al. (2007); Morbidi et al. (2016)]. Therefore, by equating the total energy supplied by the battery pack to the ideal power consumed by all the motors (8 in total), the power consumed by the motors is given by:

$$P(t) = \sum_{i=1}^{8} e_i(t) i_i(t) \tag{2.29}$$

Hence from the above equation, we can see that in order to minimize battery usage the following performance index needs to be minimized (the Lagrange type problem):

$$J = \int_0^{t_f} \sum_{i=1}^{8} e_i(t) i_i(t) dt \tag{2.30}$$

The performance index of multiphase optimal control problem for the vertical trajectory optimization of the eVTOL aircraft is as follows:

$$J = \sum_{N=1}^{2} \int_{t_0^N}^{t_f^N} \sum_{i=1}^{8} e_i(t) i_i(t) dt \tag{2.31}$$

where N is the vertical flight phase (N = 1 for cruise and N = 2 for descent). Assuming that the power supplied by the battery pack is equal to the power required (induced and parasite), ignoring the profile power, the performance index for the vertical trajectory optimization of the eVTOL aircraft is:

$$J = \sum_{N=1}^{2} \int_{t_0^N}^{t_f^N} (\sum_{i=1}^{4} (P_{arm})_i + TV \sin\alpha) dt \tag{2.32}$$

2.2.10 Path Constraints

The eVTOL aircraft's pitch angle is assumed to be bounded to 6° for passenger comfort based on discussions with experienced pilots.

$$-6^\circ \leq \theta_{fuselage} \leq 6^\circ \tag{2.33}$$

Therefore, in this research, collective pitch mechanism of a multirotor eVTOL, i.e., the collective changes to the pitch angle of the rotor-tip-path-plane of all the rotors are studied for the feasibility of a UAM mission without passenger discomfort.

The maximum speed (m/s), maximum cruise altitude (m) and total power (KW) is bounded based on specifications of EHang 184 [EHang-184 (2018)]:

$$0 \leq V_x \leq 27.78 \tag{2.34}$$

$$0 \leq h \leq 3500 \tag{2.35}$$

$$P_{required} \leq 152 \tag{2.36}$$

where $P_{required}$ is defined in equation 2.27.

When a multirotor aircraft starts to descend from the cruise phase, the flow starts to develop recirculation near the disk and turbulence above it Johnson (2012); Chenglong et al. (2015). However, at small rates of descent, the flow in the vicinity of the disk is still reasonably well represented by the momentum theory model. In vortex ring state, the flow near the rotor disk becomes highly unsteady and turbulent. Hence, the rotor in this state experiences a very high vibration level and loss of control. In order, to avoid the eVTOL aircraft entering into vortex ring state, the following

path constraint has been imposed to the descent phase of the problem Johnson (2012); Chenglong et al. (2015):

$$-0.28 \leq \frac{V \sin \alpha}{(v_h)_e} \leq 0 \tag{2.37}$$

$$(v_h)_e = \sqrt{\frac{2T_{rotor}}{2\rho A}} \tag{2.38}$$

where V is the true airspeed of the eVTOL aircraft, T_{rotor} is the thrust produced by the upper/lower rotor of the co-axial rotor system, $(v_h)_e$ is the effective induced velocity in hover of the co-axial rotor system and α is the angle of attack of the tip-path-plane of the rotors.

The bounds on the two control variables of the multiphase optimal control problem: (i) rotor tip-path-plane pitch angle (θ) and (ii) Thrust (T) are discussed in section IV.

The cruise phase transitions to descent phase at Top of Descent (TOD) waypoint. Hence, TOD i.e. phase transition waypoint is subject to the phase link constraints on state variables (y) apart from the path and control constraints [Rao et al. (2010); Garg et al. (2010)]:

$$y^{N-1}(t_f^{N-1}) = y^N(t_0^N) \tag{2.39}$$

In our initial effort, airspace restrictions on the speed and altitude of the aircraft have been ignored. However, our framework allows us to easily modify bounds on the state and control variables based on new research findings about passenger comfortability and operational requirements.

2.2.11 Fixed Final Time

The implementation of RTA in the trajectory optimization (4D) of an eVTOL aircraft would be critical to the traffic management of UAM operations in future. In UAM operation, RTAs for individual eVTOL aircraft will be calculated by arrival scheduling algorithms [Kleinbekman et al. (2018); Pradeep and Wei (2018c)]. In the current research, RTA is imposed as final time constraint on the multiphase optimal control problem for eVTOL aircraft (EHang 184). Hence, the vertical trajectory optimization problem involves fixed final time (t_f) and position [x_f, h_f].

$$t_f = RTA \tag{2.40}$$

2.3 Numerical Study

The equations of motion of the multirotor eVTOL aircraft (EHang 184) are continuous-time nonlinear differential equations which are difficult to solve analytically. For this reason, the vertical trajectory optimization problems are usually solved using direct collocation methods [Park and Clarke (2012); Dalmau et al. (2016)]. A pseudospectral is a direct collocation method that transcribes a multiphase optimal control problem to a large sparse nonlinear programming (NLP) problem [Rao et al. (2010); Garg et al. (2010)]. We used GPOPS-II [Rao et al. (2010); Garg et al. (2010)] for transcribing the multirotor eVTOL's multiphase optimal control problem for a given CONOP to the corresponding NLP using hp-adaptive Gaussian quadrature collocation. The corresponding NLP is then solved using IPOPT [Wächter and Biegler (2006); Rao et al. (2010); Garg et al. (2010)].

As GPOPS and IPOPT may find a local optimum solution instead of the global optimum solution Gauntt (2012), therefore, five different types of CONOPs are numerically studied to understand and compare different airborne delay absorption strategies. The five CONOPs are as shown in Table 2.2 and Figures 2.3, 2.4, 2.5, 2.6, 2.7. Since the airborne delay is equal to the difference between the assigned RTA and nominal time of arrival [Nikoleris et al. (2016)] for a given aircraft type and CONOP, therefore, in this dissertation assigned RTAs are varied to study the impact of the airborne delay on energy consumption by EHang 184 for different CONOPs.

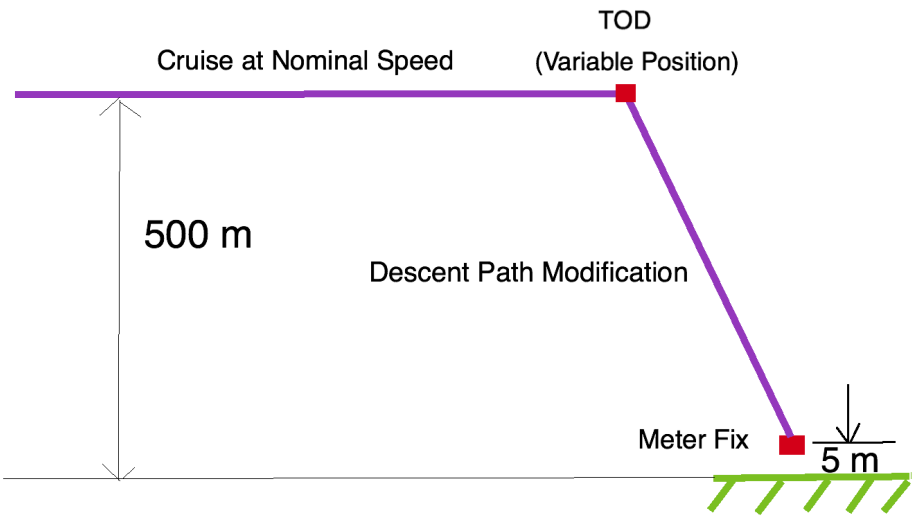

Figure 2.3: CONOP 1 (Delay Absorption by Descent Path Modification)

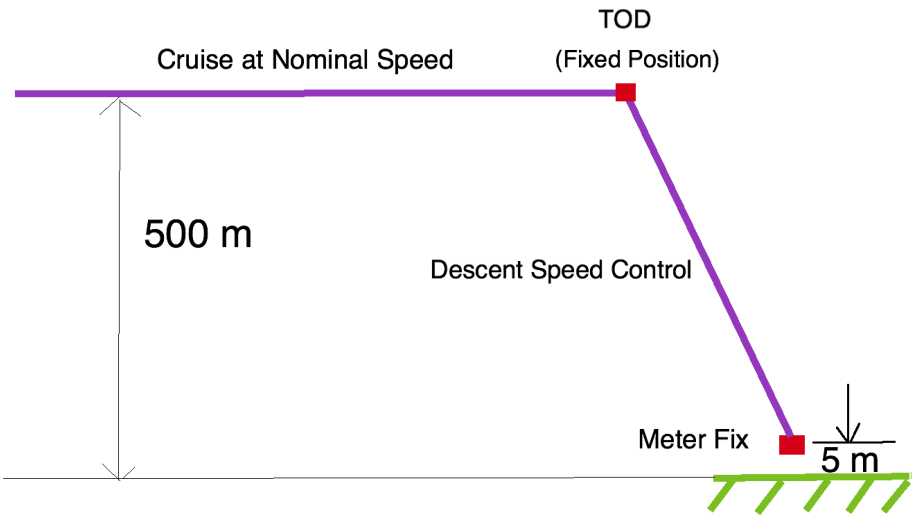

Figure 2.4: CONOP 2 (Delay Absorption by Descent Speed Control)

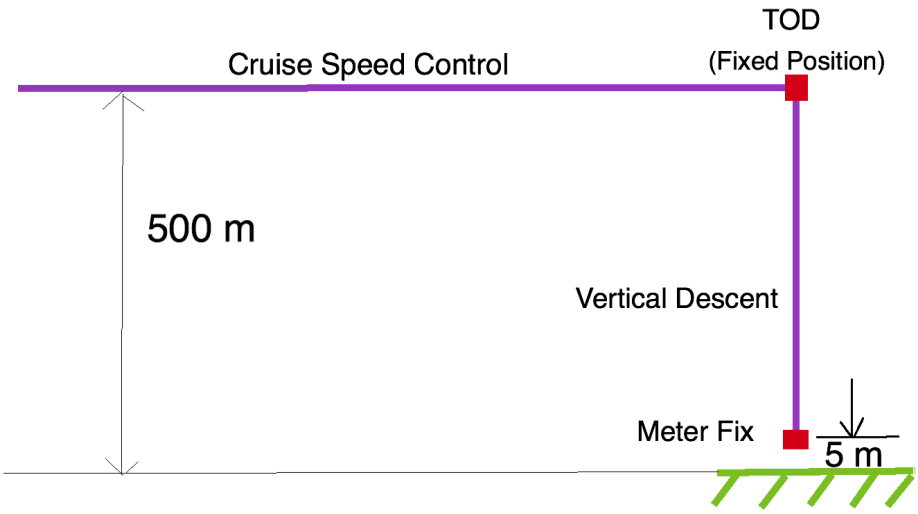

Figure 2.5: CONOP 3 (Delay Absorption by Cruise Speed Control)

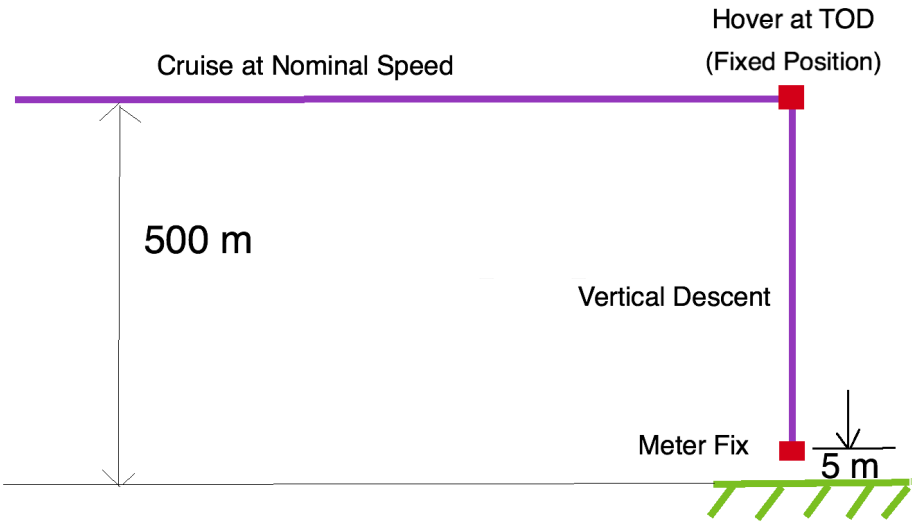

Figure 2.6: CONOP 4 (Delay Absorption by Hovering)

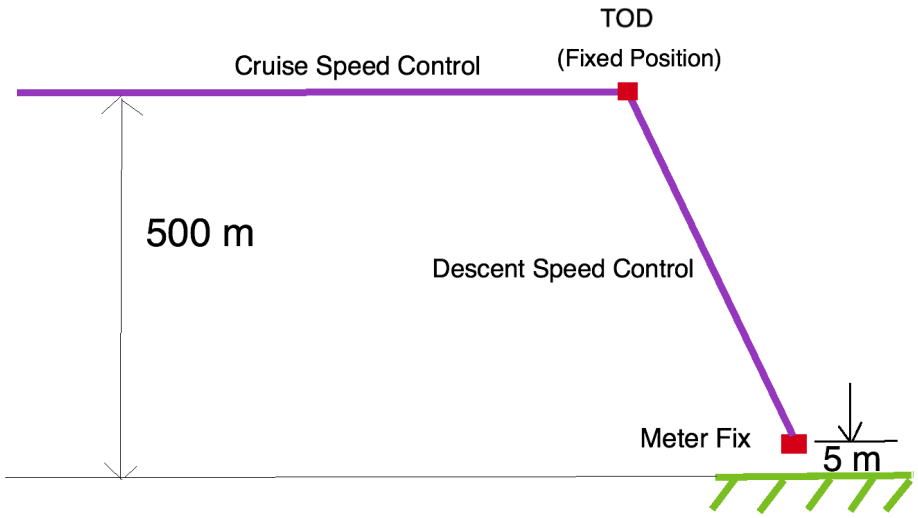

Figure 2.7: CONOP 5 (Delay Absorption Using the Combination of Cruise and Descent Speed Control)

Table 2.2: Delay Absorption Strategies (CONOPs)

CONOP	**Description**
CONOP 1	Cruise at nominal speed followed by delay absorption primarily by descent path modification (variable TOD position).
CONOP 2	Cruise at nominal speed followed by delay absorption primarily by descent speed control (adjustment). The location of TOD is fixed.
CONOP 3	Delay absorption using cruise speed control (adjustment) followed by optimized vertical descent.
CONOP 4	Cruise at nominal speed followed by delay absorption using hover at TOD and then optimized vertical descent.
CONOP 5	Delay absorption using the combination of cruise speed control (adjustment) and descent speed control (adjustment) with equal distribution of delay to both the phases. The location of TOD is fixed.

As EHang 184 is a short range and slow speed eVTOL aircraft [Uber-Elevate (2016)], the starting point for the fixed final time arrival trajectory optimization problem has been chosen as 20 km along-track distance from the vertiport. For all the CONOPs, the initial conditions (IC) and final conditions (FC) for the multiphase optimal control problem are as shown in Table 2.3. Since the initial altitude and final altitude of the eVTOL aircraft are greater than two times of rotor radius (2R), the in-ground effect (IGE) is neglected [Johnson (2012)].

Table 2.3: Initial and Final Conditions for Arrival of Multirotor eVTOL

State Variable	**IC**	**FC**
Altitude (m)	500	5
Along-track distance (m)	0	20000
Time (s)	0	RTA (t_f)

2.3.1 CONOP 1: Delay Absorption in Descent Phase (Variable TOD Position)

The first CONOP consists of cruise at nominal speed (27.78 m/s) [EHang-184 (2018)] followed by descent as shown in Figure 2.3. The location of TOD is computed by the numerical solver (GPOPS/IPOPT) of two-phase (cruise and descent) optimal control problem with fixed final time (i.e. assigned RTA). Hence, the airborne delay is mainly absorbed in descent phase by modification of the descent profile (vertical trajectory).

2.3.1.1 Energy Efficient Vertical Trajectories of the Fixed Pitch eVTOL aircraft

In this case study, the energy efficient trajectories are generated by assuming EHang 184 as a fixed pitch eVTOL aircraft. Further, the pitch angle of the fuselage of the eVTOL aircraft is assumed to be same as the pitch angle of the tip-path-plane of the rotors. Therefore, control bounds imposed on the pitch angle of the tip-path-plane of the rotors are based on passenger comfort ($-6^\circ \leq \theta_{fuselage} \leq 6^\circ$) as shown in Table 2.4.

Table 2.4: Lower and Upper Bounds on Control Variables (Fixed Pitch)

Control Variable	Lower Bound	Upper Bound
Rotor Pitch Angle (deg)	-6	6
Thrust (N)	0	4800

Figure 2.8, shows that for the energy efficient trajectories of CONOP 1, the airborne delays are progressively absorbed by shortening of the cruise segment followed by flying a shallower descent (i.e., TOD is computed further away from the destination) to meet the assigned RTAs. The sharp increase or decrease in control variables during the vertical phase transition in Figure 2.9, can be attributed to the problem formulation assumption of quasi-steady flight with point mass model for the eVTOL aircraft and numerical error due to using a less accurate numerical method, i.e., direct collocation method to solve the multiphase optimal control problem.

From Figure 2.8 and Figure 2.9, it can also be inferred that the lower and upper control bounds of +/- 6 degrees on the rotor pitch angle are insufficient to fly at 27.78 m/s, i.e., nominal cruise

speed of EHang 184. As the results (computed cruise ground speeds) of the fixed pitch eVTOL aircraft is not in adherence to the proposed CONOP 1 for different RTAs, therefore, the results of this case study (fixed pitch mechanism) are not considered for energy consumption analysis. Thus, all onward case studies are carried out assuming that the eVTOL aircraft (EHang 184) has a collective pitch mechanism.

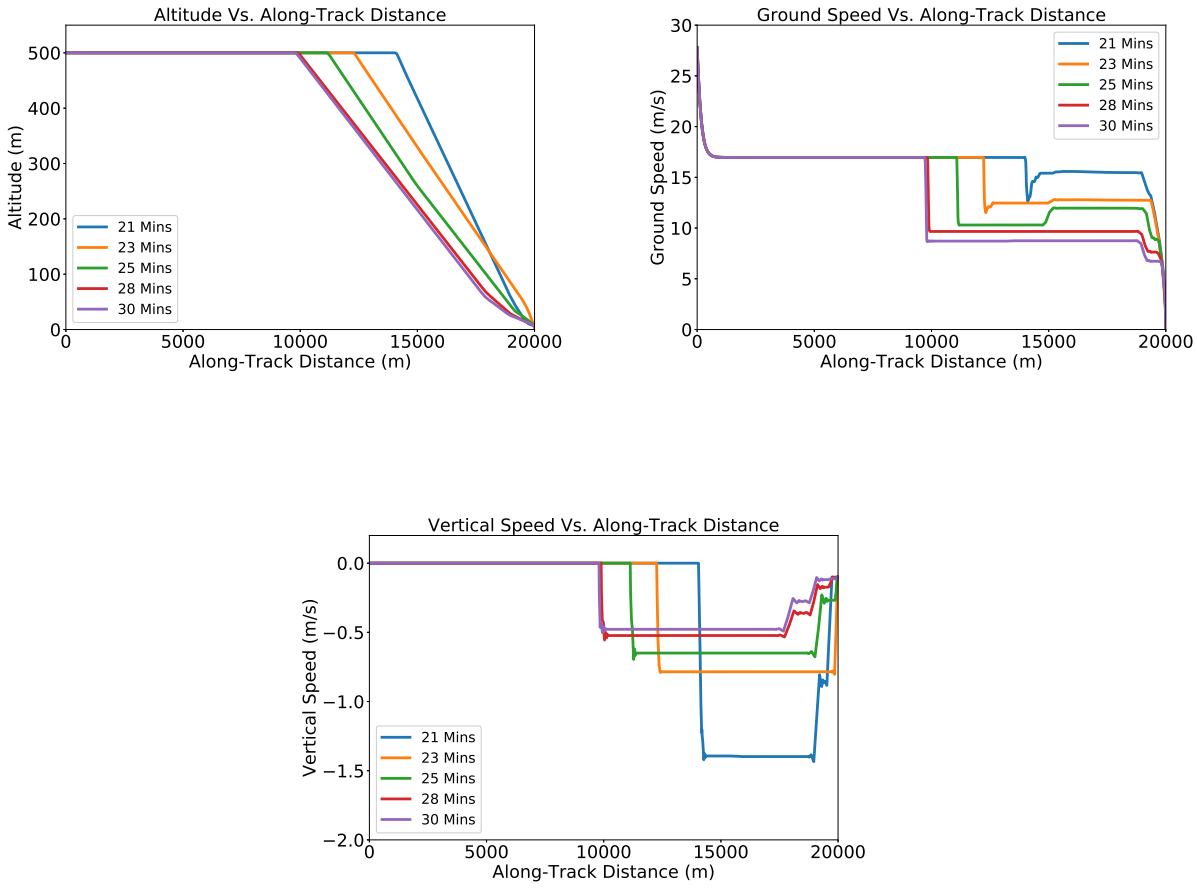

Figure 2.8: CONOP 1: Energy Efficient Altitude, Ground Speed and Vertical Speed Profiles of the Fixed Pitch eVTOL Aircraft under Various RTAs

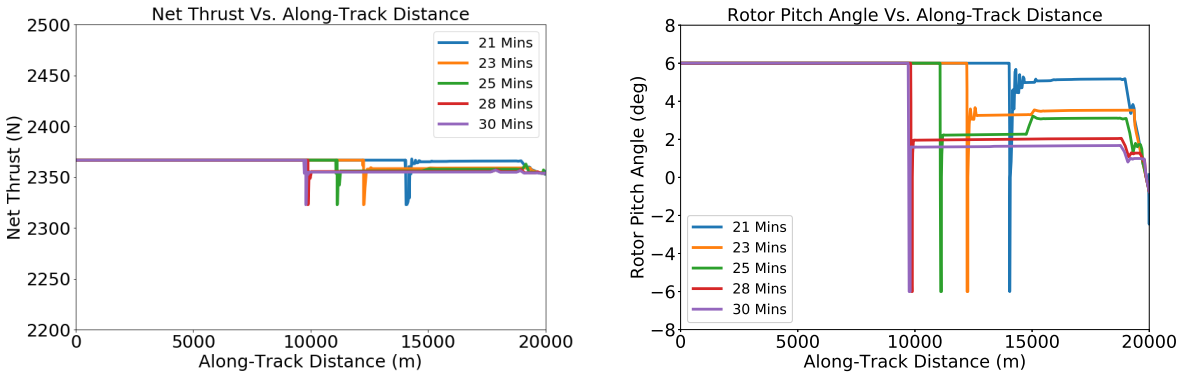

Figure 2.9: CONOP 1: Energy Efficient Control Strategy of the Fixed Pitch eVTOL Aircraft under Various RTAs

2.3.1.2 Energy Efficient Vertical Trajectories of the Collective Pitch eVTOL aircraft

As stated earlier, in this case study, the results are generated assuming the eVTOL aircraft has a collective pitch mechanism. Therefore, control bounds are not imposed on the pitch angle of the tip-path-plane of the rotors based on the passenger comfort as shown in Table 2.5.

Table 2.5: Lower and Upper Bounds on Control Variables (Collective Pitch)

Control Variable	Lower Bound	Upper Bound
Rotor Pitch Angle (deg)	-25	25
Thrust (N)	0	4800

Unlike the previous case study, the ground speed for the cruise segment is computed as 27.78 m/s, i.e., EHang 184's nominal cruise speed. Therefore, Figure 2.11 and Figure 2.12 suggest that the collective pitch mechanism is required for the operational feasibility of a multirotor eVTOL aircraft like EHang 184 considering passenger comfort.

Figure 2.11, shows that for the energy efficient trajectories of CONOP 1; the airborne delays are progressively absorbed by shortening of the cruise segment followed by flying a shallower descent

(i.e., TOD is computed further away from the destination) to meet the assigned RTAs. From Figure 2.13, it can be seen that with an increase in the airborne delays (assigned RTAs) the energy consumption is distributed more on to the descent phase than the cruise phase for CONOP 1. Therefore, the results of CONOP 1 show the advantage of using a shallower descent path (descent path modification strategy) for the airborne delay absorption.

As stated before, the sharp increase or decrease in control variables during the vertical phase transition can be attributed to the problem formulation assumption of quasi-steady flight with point mass model for the eVTOL aircraft and numerical error due to using a less accurate numerical method, i.e., direct method to solve the multiphase optimal control problem.

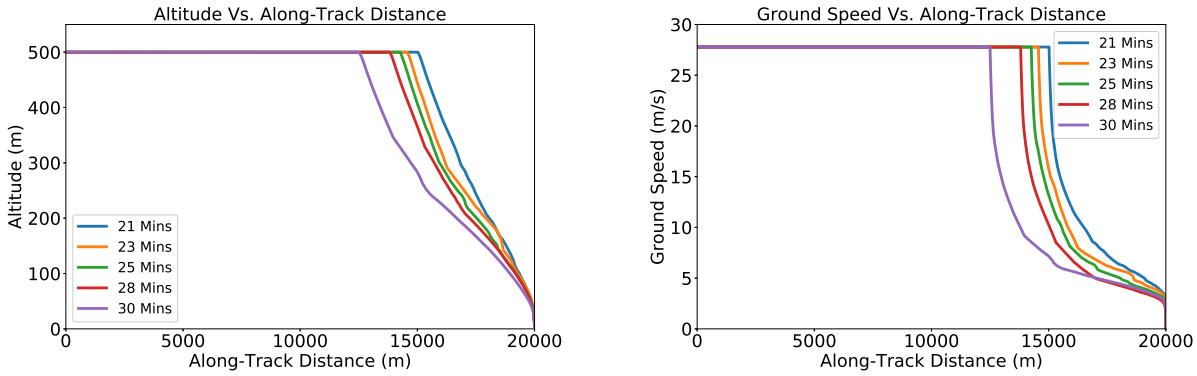

Figure 2.10: CONOP 1: Energy Efficient Altitude and Ground Speed Profiles of the Collective Pitch eVTOL Aircraft under Various RTAs

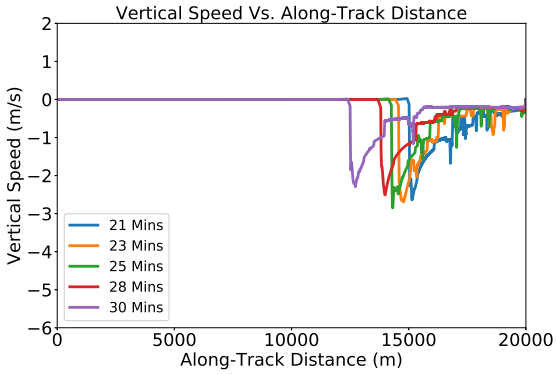

Figure 2.11: CONOP 1: Energy Efficient Vertical Speed Profile of the Collective Pitch eVTOL Aircraft under Various RTAs

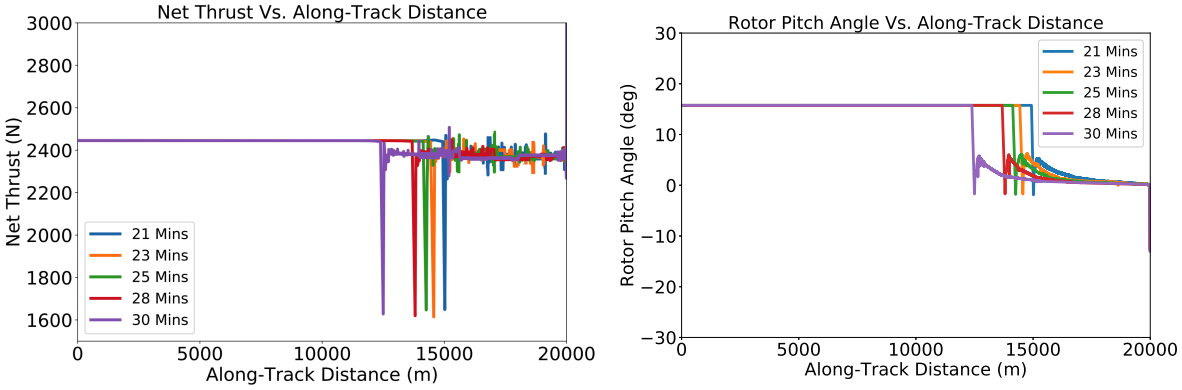

Figure 2.12: CONOP 1: Energy Efficient Control Strategy of the Collective Pitch eVTOL Aircraft under Various RTAs

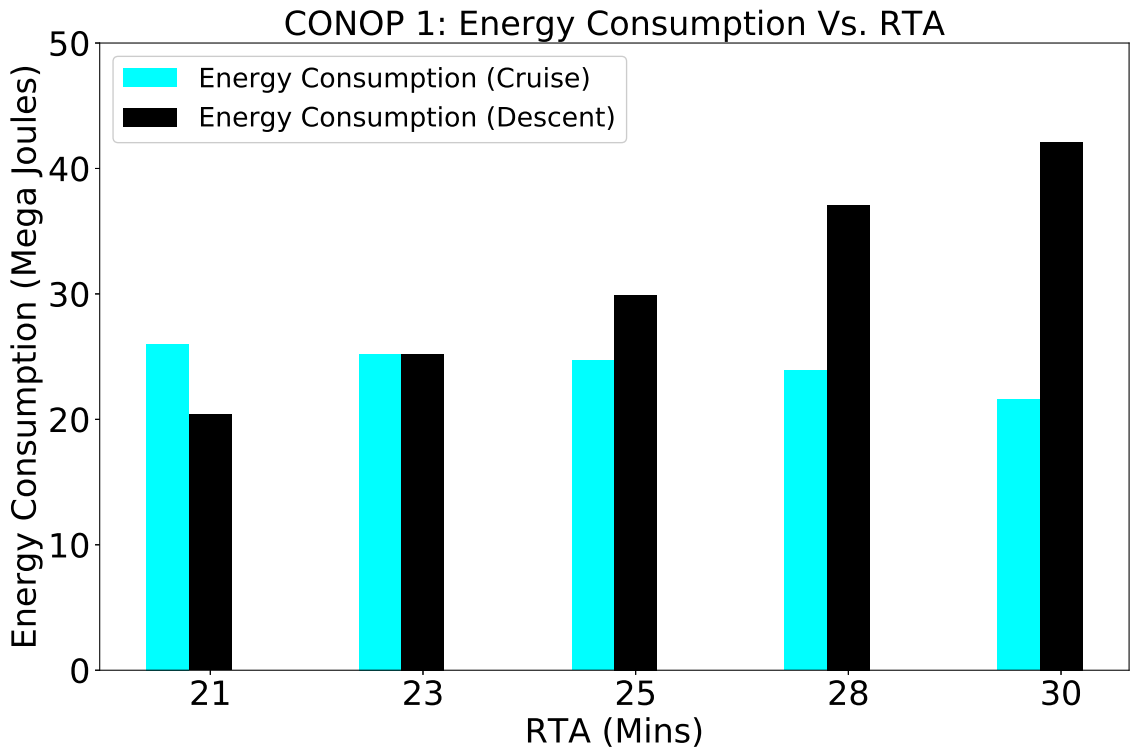

Figure 2.13: CONOP 1: Energy Consumption in Cruise and Descent Phases under Various RTAs

2.3.2 CONOP 2: Delay Absorption in Descent Phase (Fixed TOD Position)

The second CONOP consists of cruise at nominal speed (27.78 m/s) [EHang-184 (2018)] followed by a shallow descent from fixed TOD position as shown in Figure 2.4. The position of TOD is calculated at cruise altitude based on descent flight path angle of 3 degrees propagating in a backward direction from the meter fix (5 m above the vertiport). The numerical solver (GPOPS/IPOPT) is used to compute the descent profile (path and speed) to meet the assigned RTA. As stated earlier, in this case study, the energy efficient trajectories are generated by assuming EHang 184 has a collective pitch mechanism. From Figure 2.14, it can be seen that for CONOP 2, the airborne delay is efficiently absorbed primarily using descent speed control (adjustment) along with minor vertical path modification between the two fixed waypoints, i.e., TOD and the meter fix. Figure 2.15, indicates that with an increase in the airborne delays (assigned RTAs) the energy consump-

tion in the descent phase increases whereas the energy consumption in the cruise phase remains the same as expected because of nominal cruise speed and fixed TOD position.

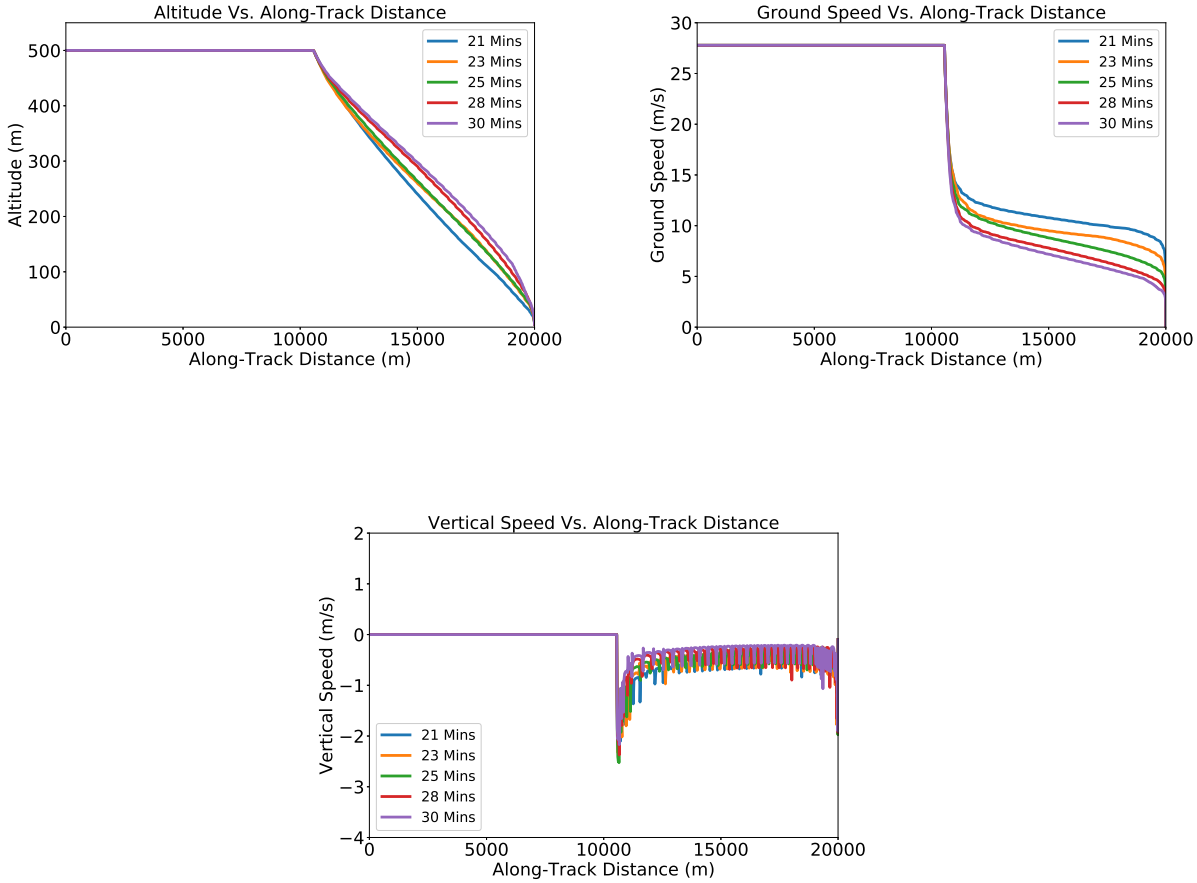

Figure 2.14: CONOP 2: Energy Efficient Altitude, Ground Speed and Vertical Speed Profiles of the Collective Pitch eVTOL Aircraft under Various RTAs

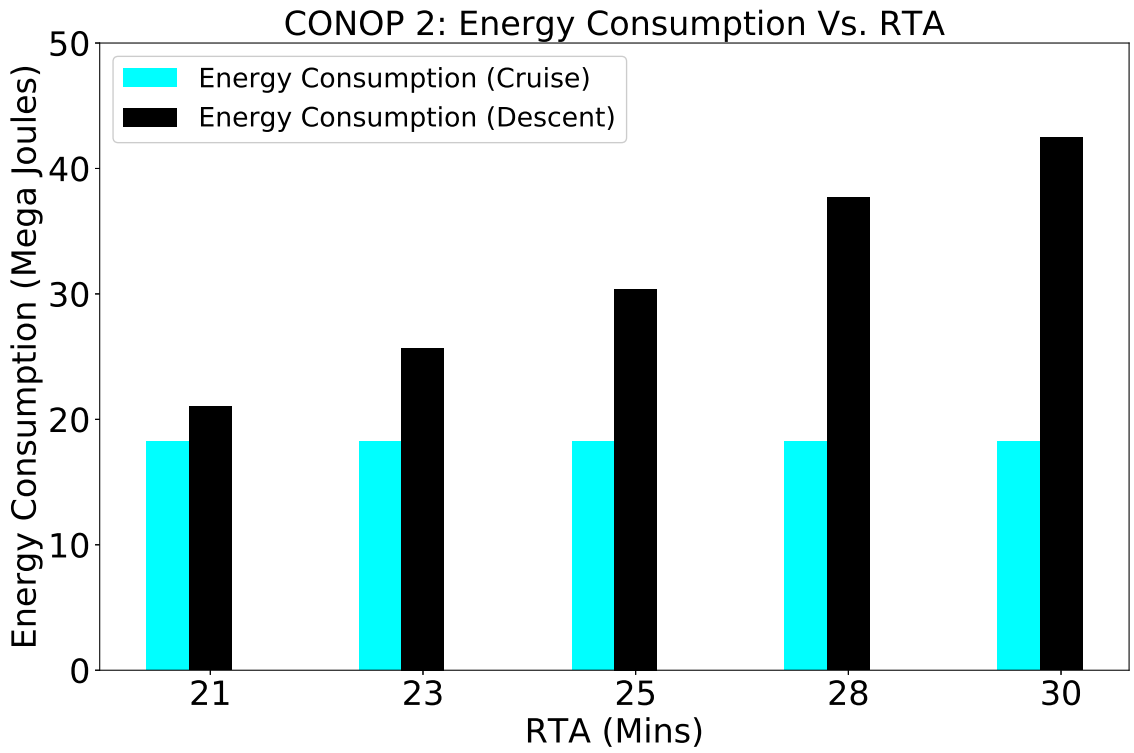

Figure 2.15: CONOP 2: Energy Consumption in Cruise and Descent Phases under Various RTAs

2.3.3 CONOP 3: Delay Absorption in Cruise Phase by Cruise Speed Control

The third CONOP consists of cruise at constant altitude followed by vertical descent as shown earlier in Figure 2.5. In this case study, only cruise speed is adjusted to absorb the airborne delay. Hence, to compute cruise profile: (i) first, the flight duration (165.02 sec) for vertical descent from cruise altitude to the meter fix is computed using a single phase optimal control framework with energy as the performance index; and (ii) then the computed flight duration for vertical descent is imposed as time constraint on the descent phase of multiphase optimal control problem for all RTAs to generate trajectories. The following RTAs to the meter fix are imposed on the eVTOL: 21, 23, 25, 28 and 30 minutes. In this case study, the results are generated assuming the eVTOL aircraft has a collective pitch mechanism.

From Figure 2.16 and Figure 2.17, it can be seen that for CONOP 3, the airborne delays, i.e., increase in RTAs (21, 23, 25, 28 and 30 minutes) are energy efficiently absorbed by controlling the

cruise speed without impacting the descent phase. Therefore, as shown in Figure 2.17, with an increase in the airborne delay (RTA) the energy consumption in the cruise phase increases while the energy consumption in the descent phase remains the same.

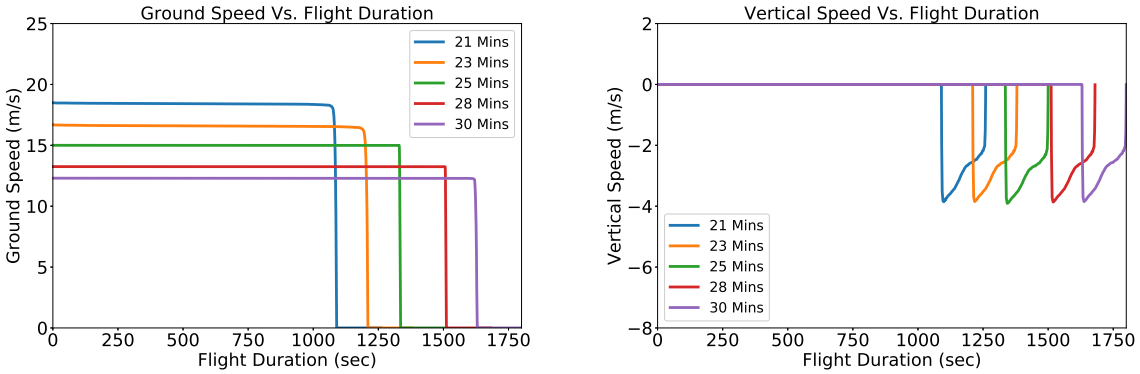

Figure 2.16: CONOP 3: Time History of Ground Speed and Vertical Speed of the Collective Pitch eVTOL Aircraft under Various RTAs

2.3.4 CONOP 4: Delay Absorption in Hover at Cruise Altitude

The fourth CONOP consists of cruise at constant altitude and nominal speed (unlike cruise speed adjustment in CONOP 3) followed by the transition to hover at TOD to absorb the airborne delay and then vertical descent as shown in Figure 2.6. In this case study, only hover time is adjusted to absorb the airborne delay. Hence to compute hover time: (i) first, the flight duration (165.02 sec) for vertical descent from cruise altitude to the meter fix is computed using a single phase optimal control framework with energy as the performance index; (ii) next, the flight duration for the cruise phase is calculated assuming cruise at constant altitude and nominal cruise speed followed by the transition to hover at TOD; and (iii) finally, the computed flight durations for vertical descent and cruise are imposed as time constraints on the descent and cruise phases of multiphase optimal control problem to compute the hover time for a given RTA. The following RTAs to the meter fix are imposed on the eVTOL: 21, 23, 25, 28 and 30 minutes. In this case

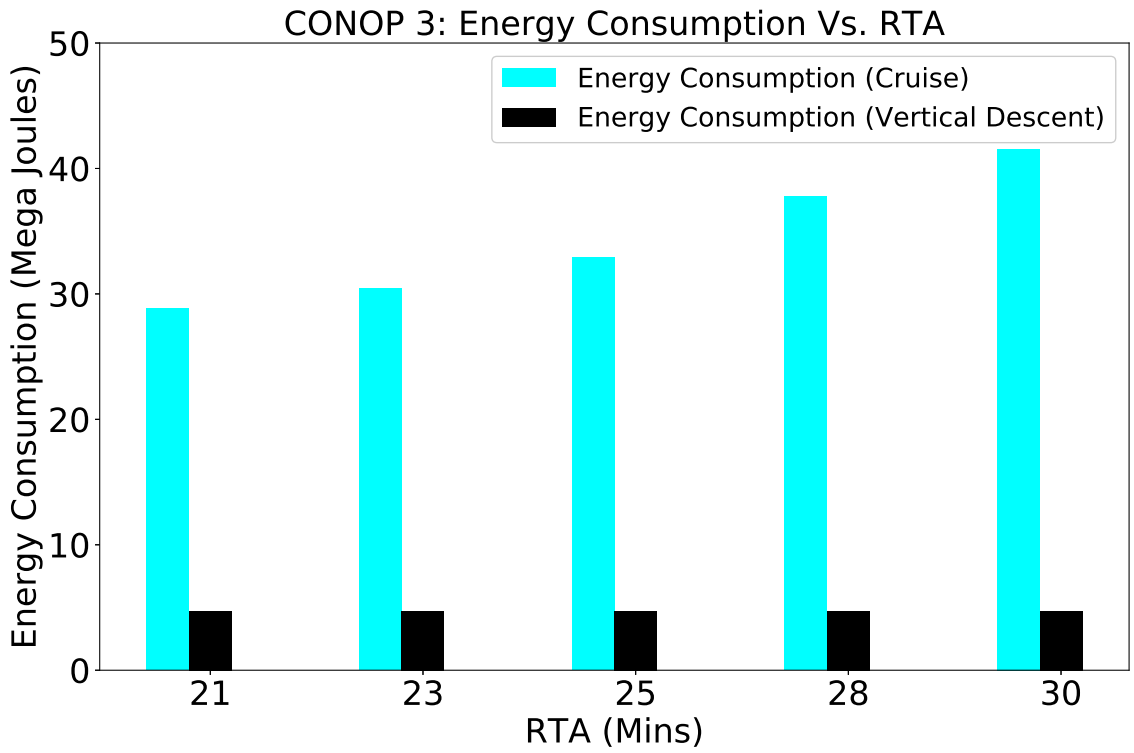

Figure 2.17: CONOP 3: Energy Consumption in Cruise and Vertical Descent Phases under Various RTAs

study, the results are generated assuming the eVTOL aircraft has a collective pitch mechanism.

From Figure 2.18, it can be seen that for CONOP 4, the airborne delay, i.e., increase in RTA (21, 23, 25, 28 and 30 minutes) is progressively absorbed in hover without impacting the cruise and descent phases. Therefore, as shown in Figure 2.18, with an increase in the airborne delay (RTA) the energy consumption in hover phase increases while the energy consumption in the cruise and descent phases remain the same.

2.3.5 CONOP 5: Delay Absorption Using the Combination of Cruise and Descent Speed Control

The fifth CONOP consists of cruise at constant altitude followed by a shallow descent from fixed TOD position as shown in Figure 2.7. The position of TOD is calculated at cruise altitude

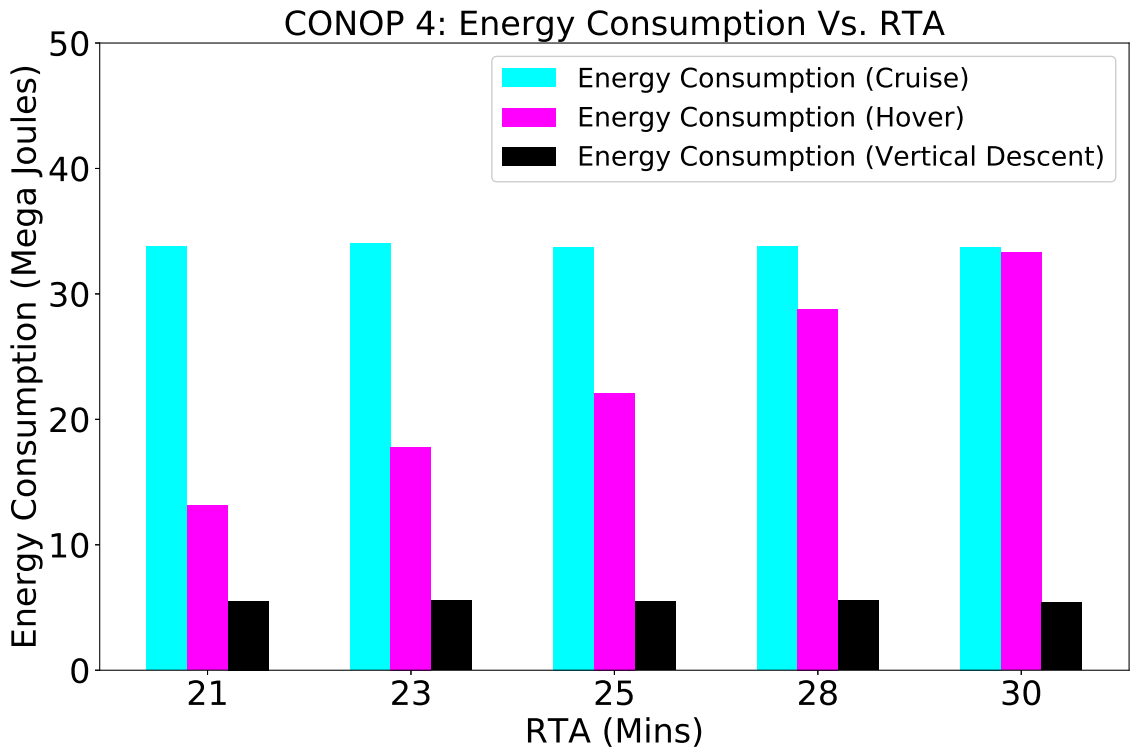

Figure 2.18: CONOP 4: Energy Consumption in Cruise, Hover and Vertical Descent Phases under Various RTAs

based on descent flight path angle of 3 degrees propagating in a backward direction from the meter fix (5 m above the vertiport). In this CONOP, the strategy is to equally distribute the airborne delay (assigned RTA) to both the phases. This strategy involves the combination of cruise speed control (adjustment) and descent speed control (adjustment) to absorb the airborne delay with minor vertical path modification between the two fixed waypoints (TOD and meter fix).

From Figure 2.19, it can be seen that for CONOP 5, the airborne delays, i.e., increase in RTAs (21, 23, 25, 28 and 30 minutes) are energy efficiently absorbed by controlling both the cruise speed and descent speed without much impact on the descent path. Therefore, as shown in Figure 2.20, with an increase in the airborne delay (assigned RTA) the energy consumption increases simultaneously in both the phases (cruise and descent).

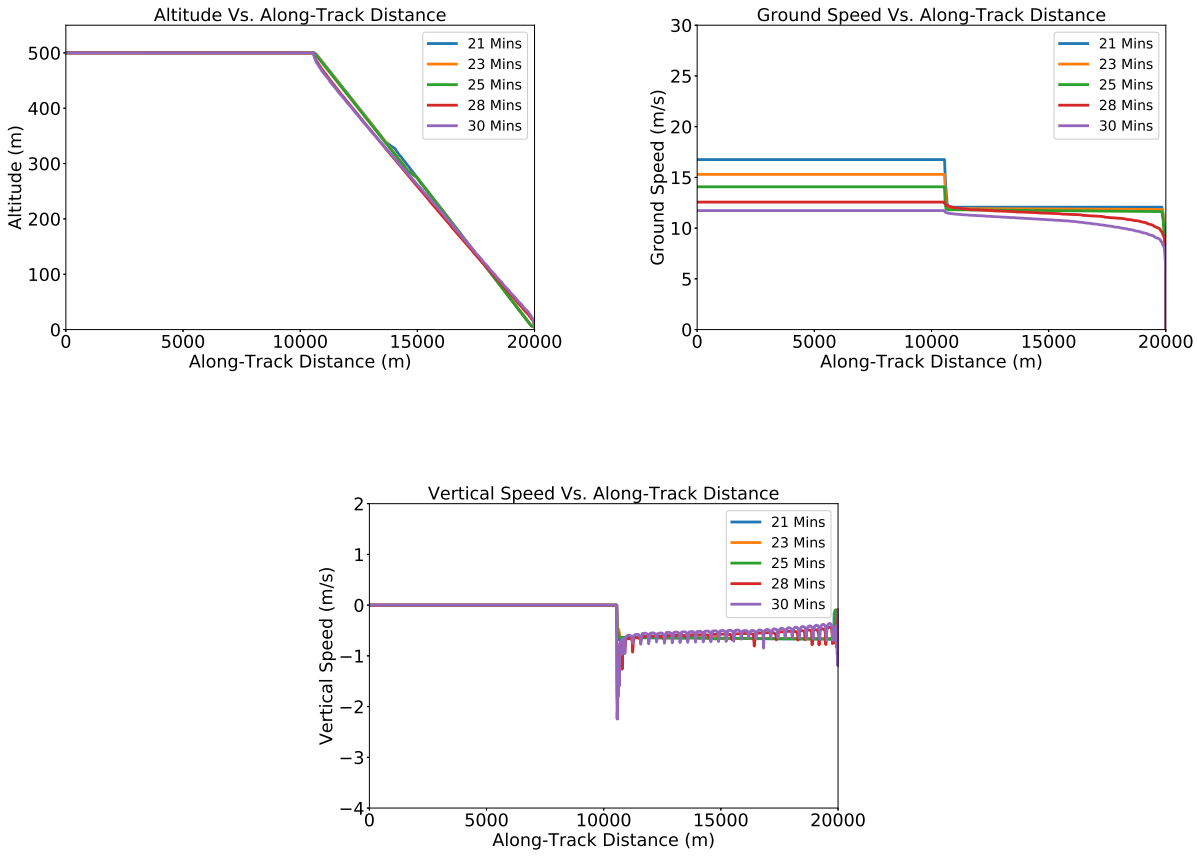

Figure 2.19: CONOP 5: Energy Efficient Altitude, Ground Speed and Vertical Speed Profiles of the Collective Pitch eVTOL Aircraft under Various RTAs

2.3.6 Comparison of Total Energy Consumptions

From Figure 2.21, it can be observed that of the five CONOPs: (i) the least total energy consumption occurs in CONOP 5, i.e., the airborne delay absorption using the combination of cruise speed control and descent speed control with a shallow descent path to the meter fix; and (ii) the highest total energy consumption occurs in CONOP 4, i.e., the airborne delay absorption by hovering at TOD. Figure 2.21 also indicates that with an increase in flight duration there is an increase in the total energy consumption for all the CONOPs and therefore a clear need for higher stored energy in onboard Li-Po batteries of the eVTOL aircraft.

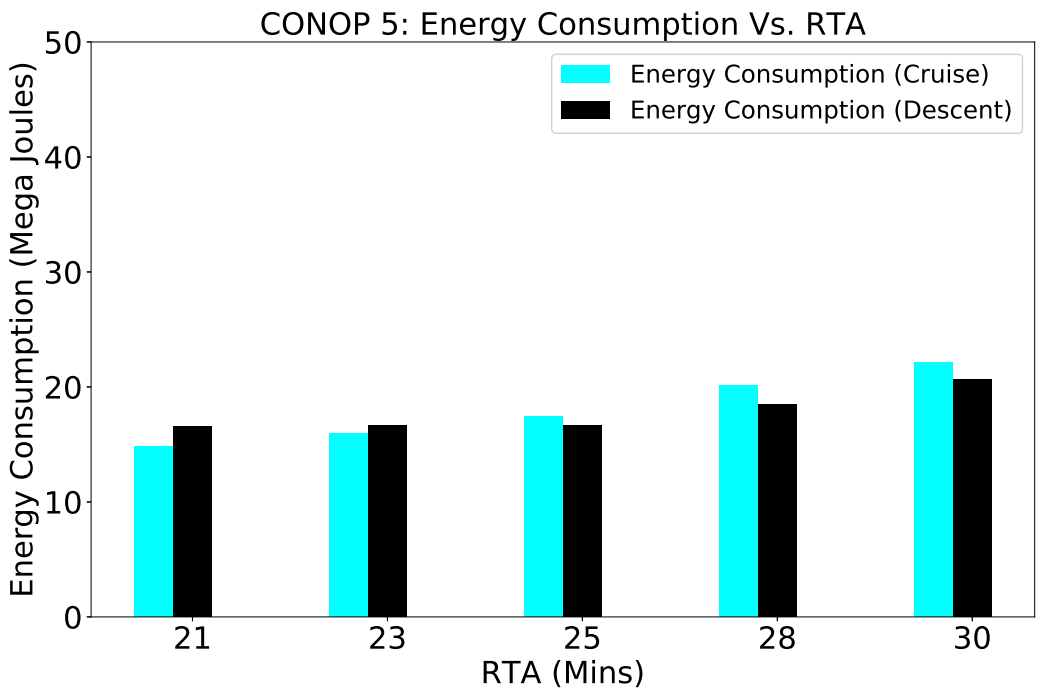

Figure 2.20: CONOP 5: Energy Consumption in Cruise and Descent Phases under Various RTAs

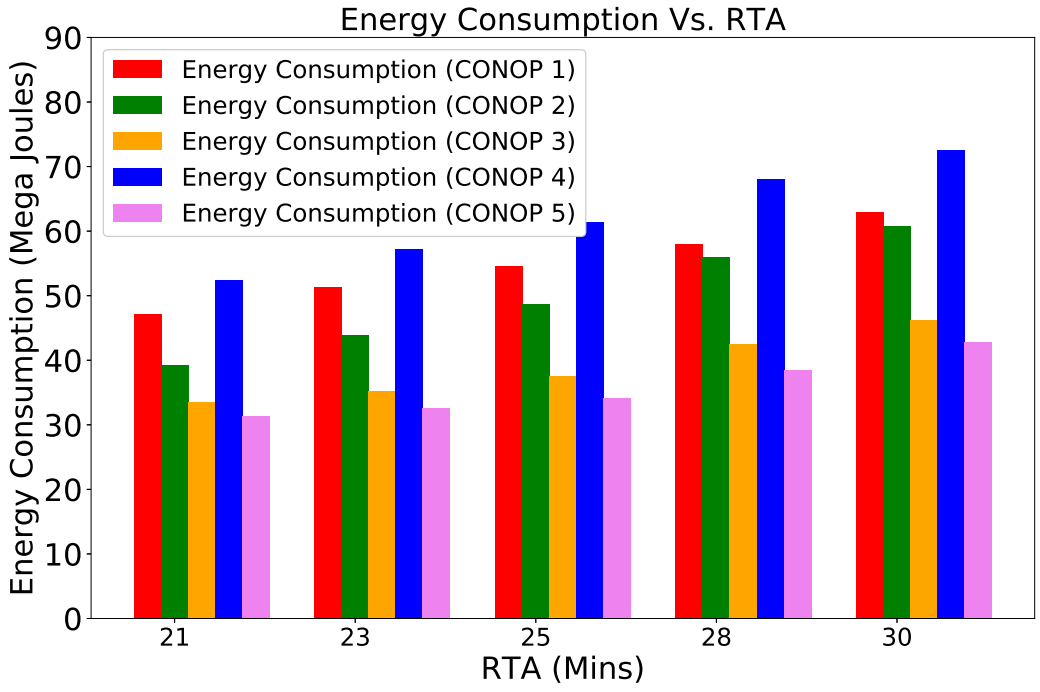

Figure 2.21: Comparison of Energy Consumption for Different CONOPs

2.4 Conclusion

In this chapter of the dissertation, multiphase optimal control problem with energy consumption as the performance index is formulated for a multirotor eVTOL aircraft (like CityAirbus, EHang 184 and Volocopter 2X) on an urban air mobility (UAM) passenger transportation mission. Further, we present a framework to perform energy efficient arrival for a multirotor eVTOL aircraft to meet the assigned required time of arrival (RTA) constraint in UAM for a given concept of operation (CONOP). The proposed framework can also be used to address an energy efficient cargo delivery case in a UAS traffic management (UTM) context.

The formulated vertical trajectory optimization problem is numerically solved using the pseudospectral method for a specific multirotor eVTOL aircraft, i.e., EHang 184 and five different types of CONOPs. The numerical results of the fixed pitch case study suggest that the collective pitch mechanism is required for the operational feasibility of a multirotor eVTOL aircraft like EHang 184 considering passenger comfort. Further, by imposing various arrival time constraints on the eVTOL aircraft, we found that for the energy efficient arrival operations, the airborne delay is best absorbed by CONOP 5, i.e., the combination of cruise speed control and descent speed control with a shallow descent path to the meter fix. The airborne delay absorption by hovering (CONOP 4) at the cruise altitude is the least energy efficient of all. Also, the numerical solutions showed that with an increase in flight duration there is an increase in the total energy consumption and therefore a clear need for higher stored energy in onboard Li-Po batteries of the eVTOL aircraft.

CHAPTER 3. ENERGY EFFICIENT ARRIVAL OF TANDEM TILT-WING EVTOL

3.1 Introduction

In this chapter of the dissertation, multiphase optimal control framework for a tandem tilt-wing eVTOL aircraft(like Airbus Vahan) [Airbus-A^3 (2018)] to perform energy efficient arrival with required time of arrival (RTA) constraint for a given concept of operation (CONOP) is presented.

3.2 Multiphase Optimal Control Problem Formulation

3.2.1 eVTOL Aircraft Model

In this chapter, the aircraft dynamics are modeled based on the tandem tilt-wing eVTOL (Airbus Vahana) from Airbus A^3 [Airbus-A^3 (2018)]. This eVTOL aircraft has two tandem tilt-wings with eight rotors as shown in Figure 3.1. The CONOP [Airbus-A^3 (2018)] used for the vertical trajectory optimization is as shown in Figure 3.2.

The performance data of the eVTOL aircraft are as shown in Table 3.1 based on design range of 60 km [Airbus-A^3 (2018)].

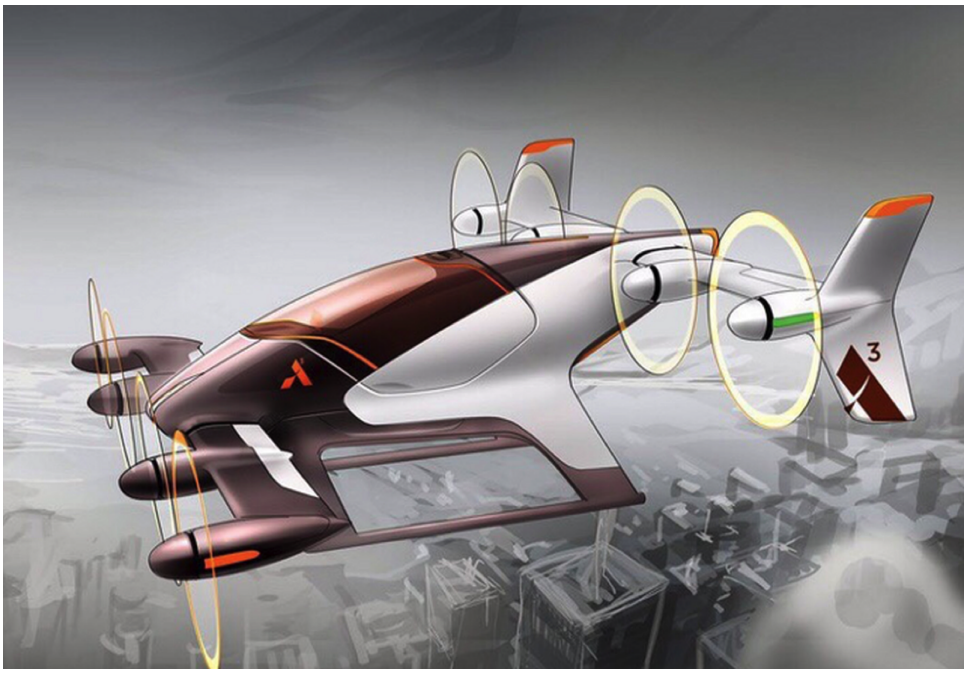

Figure 3.1: Airbus Vahana: Tandem Tilt-Wing Configuration During the Cruise Phase [Airbus-A^3 (2018)]

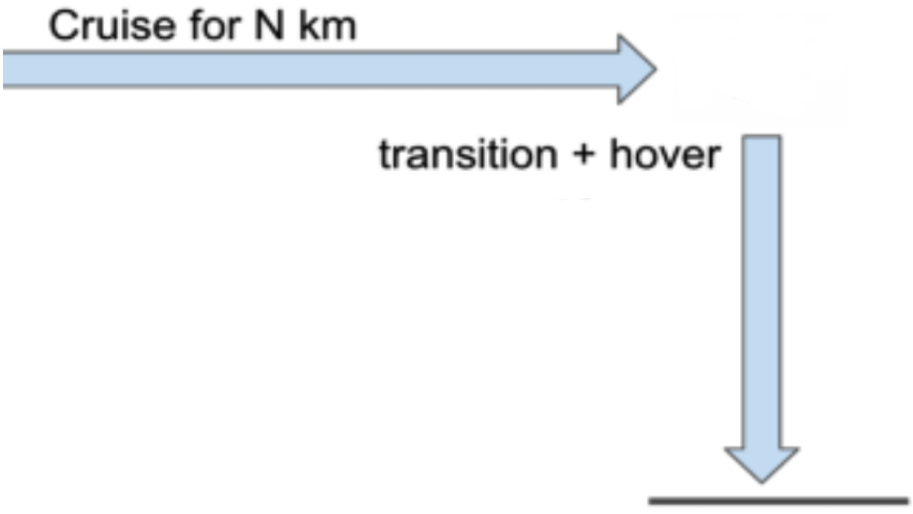

Figure 3.2: Vertical Trajectory of the eVTOL's Arrival [Airbus-A^3 (2018)]

Table 3.1: Performance Data of Airbus Vahana [Airbus-A^3 (2018)]

Performance Parameter	**Value**
m	752.2 kg
b_{ref}	6.87 m
S_{ref}	8.93 m^2
AR	5.29
e	1.3
c_{ref}	0.65 m
$(C_{D0})_{wing}$	0.012
$(C_{D0})_{fuselage}$	0.039
$(\frac{L}{D})_{cruise}$	5.92
η_{prop}	0.8
F_{top}	5.8 m^2
R	0.95 m
V_{stall}	35 m/s
$V_{max\ cruise}$	80 m/s

3.2.2 Trajectory Optimization

In this research, the longitudinal flight dynamics for the tandem tilt-wing aircraft are decoupled from the lateral flight dynamics as the eVTOL has a symmetrical: i) wing structure and ii) placements of rotors about the longitudinal axis; like fixed-wing aircraft and quadrotors respectively. Hence, the decoupling logic used by researchers for fixed-wing aircraft [Rivas et al. (2013); Stell (2011); Park and Clarke (2012); Pradeep and Wei (2017); Falck et al. (2017)], conventional rotorcraft [Johnson (2012, 1977); Bottasso et al. (2005); Yomchinda et al. (2011)] and quadrotors [Pradeep and Wei (2018a); Pradeep et al. (2018)] are assumed to be applicable for the tandem tilt-wing eVTOL as well.

In this dissertation, the following assumptions have been made:

- The lateral trajectory is a geodesic path.
- The vertical trajectory of arrival consists of a portion of the cruise, transition, and descent phases.
- Only, a part of the cruise phase is considered to study energy efficient delay absorption while airborne.
- The transition phase involves tandem tilt of rotors and wings for the transition from cruise speed to hover for the vertical descent per the concept of operation (CONOP) of Airbus Vahana [Airbus-A^3 (2018)].
- In the transition phase, the rotation of rotors and wings from cruise to vertical descent configuration occurs in negligible time with ignorable mechanical energy losses.
- The transition phase, consists of the following sub-phases: i) deceleration to hover speed and ii) hover above the vertiport at the cruise altitude.
- The descent phase includes vertical descent.

Therefore, only the speed profile of the eVTOL aircraft is free for the optimization. However, since the arrival time constraint has been imposed on the eVTOL aircraft, the trajectory optimization problem involves computation of an energy efficient speed profile for the eVTOL aircraft with fixed final time [Pradeep and Wei (2018a)].

3.2.3 Cruise Flight Dynamics

The decoupling of the longitudinal and lateral flight dynamics allows us to solve the vertical trajectory generation problem as a two-dimensional flight dynamics problem in the vertical plane. Therefore, the equations of motion for the tandem tilt-wing eVTOL aircraft (shown in Figure 3.3)

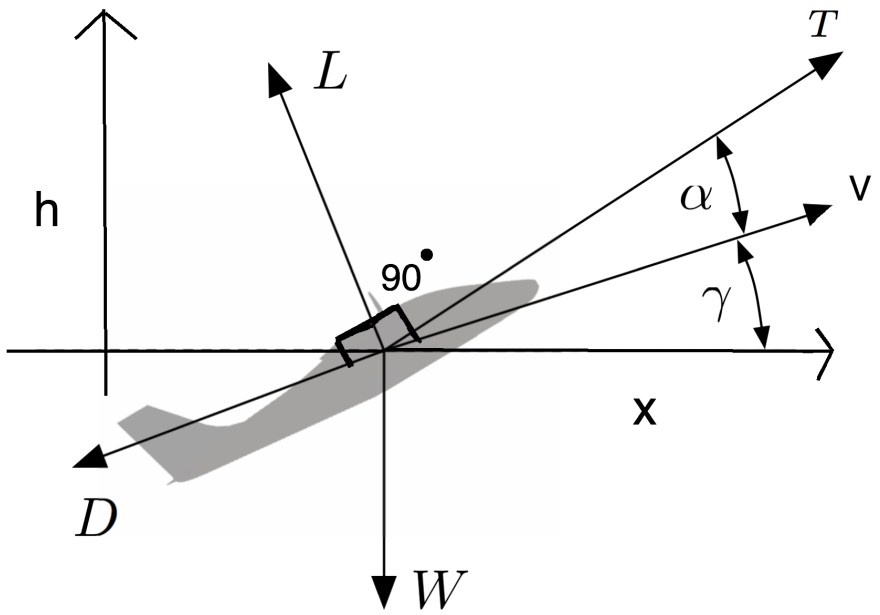

Figure 3.3: Free Body Diagram of the eVTOL Aircraft [Falck et al. (2017)]

in aerodynamic frame of reference are as follows [Rivas et al. (2013); Stell (2011); Park and Clarke (2012); Pradeep and Wei (2017); Falck et al. (2017)]:

$$\frac{dV}{dt} = \frac{T\cos\alpha - D - W\sin\gamma}{m} \tag{3.1}$$

$$\frac{dx}{dt} = V\cos\gamma \tag{3.2}$$

$$\frac{dh}{dt} = V\sin\gamma \tag{3.3}$$

$$T = \sum_{i=1}^{8} T_i \tag{3.4}$$

where $[x, h]$ is the position vector (along track distance, altitude) of the center of mass relative to the initial position, α is the angle between the thrust vector and the aerodynamic velocity, γ is the aerodynamic flight path angle, T is the net thrust produced by DEP of the eVTOL, D is the net drag, L is the net Lift, T_i is the thrust produced by the i^{th} rotor, m is the mass, V is the true airspeed, W is the weight of the eVTOL aircraft and g is the acceleration due to gravity.

3.2.4 Path Constraints in Cruise Phase

The path constraints for the tandem tilt-wing eVTOL aircraft in the cruise phase are as follows:

i) Assuming the cruise phase consists of constant level flight segments:

$$T \sin \alpha + L - W \cos \gamma = 0 \tag{3.5}$$

$$\frac{dh}{dt} = 0 \tag{3.6}$$

$$\gamma = 0 \tag{3.7}$$

ii) Lower and upper bounds on the cruise speed:

$$1.3V_{stall} \leq V \leq V_{max\ cruise} \tag{3.8}$$

3.2.5 Drag Model in Cruise

The cruise performance of the tandem tilt-wing eVTOL aircraft is based on a traditional quadratic drag polar with a span efficiency factor (e) of 1.3 [Airbus-A^3 (2018)]. The drag model used in this research is based on Airbus Vahana's drag model as follows [Airbus-A^3 (2018)]:

$$S_{ref} = \frac{2L}{\rho V_{stall}^2 C_{Lmax}} \tag{3.9}$$

where $C_{Lmax} = 1.1$, $V_{stall} = 35$ m/s, ρ is the density of air at the cruising altitude and S_{ref} is the reference area of the eVTOL (both wings combined).

$$AR = \frac{b_{ref}^2}{S_{ref}} \tag{3.10}$$

where AR is the equivalent aspect ratio of the eVTOL aircraft.

$$C_{D0} = (C_{D0})_{wing} + (C_{D0})_{fuselage} \tag{3.11}$$

where C_{D0} is the overall parasite drag coefficient based on the lumped drag model.

$$L = \frac{\rho V^2 S_{ref} C_L}{2} \tag{3.12}$$

where L is the lift, C_L is the coefficient of lift and V is the true airspeed.

$$D = \frac{\rho V^2 S_{ref}}{2}(C_{D0} + \frac{C_L^2}{\pi ARe}) \tag{3.13}$$

where D is the net drag, AR is the aspect ratio and e is the span efficiency.

3.2.6 Power Consumption Model in Cruise

The power consumption model by DEP of the eVTOL aircraft in cruise phase is derived from the standard lift, drag, and propulsion models assuming quasi-steady and constant altitude of the aircraft [Klesh and Kabamba (2009)]. The equation governing the power consumption by DEP of the tandem tilt-wing eVTOL aircraft in cruise phase is as follows [Klesh and Kabamba (2009)]:

$$P = \frac{TV\cos\alpha}{\eta_{prop}} \tag{3.14}$$

where T is the net thrust produced by DEP of the eVTOL, η_{prop} is the efficiency of the propeller, α is the angle between the thrust vector and the aerodynamic velocity and V is the true air speed of the eVTOL aircraft.

Therefore, the total energy consumed (E_{cruise}) by DEP in cruise phase is as follows:

$$E_{cruise} = \int_0^{t_f^{cruise}} P dt \tag{3.15}$$

3.2.7 Transition Flight Dynamics

In the transition phase, the eVTOL is assumed to decelerate from cruise speed to hover at a constant altitude [Airbus-A^3 (2018)]. Hence, transition phase consists of deceleration of the eVTOL followed by hover above the vertiport at the cruise altitude. In this research, we have assumed the following: i) rotation of wings and rotors from cruise configuration (Figure 3.1) to vertical descent configuration (Figure 3.4) occurs in negligible duration of time and ii) deceleration of the eVTOL aircraft occurs solely due to the aerodynamic drag. Hence, the equations of motion in transition phase is given by:

$$\frac{dV}{dt} = -\frac{D}{m} \tag{3.16}$$

$$\frac{dx}{dt} = V \tag{3.17}$$

$$T = \sum_{i=1}^{8} T_i \tag{3.18}$$

3.2.8 Path Constraints in Transition Phase

The path constraints for the tandem tilt-wing eVTOL aircraft in transition phase are as follows:

i) Assuming transition phase consisting of constant level flight segments:

$$T - W = 0 \tag{3.19}$$

$$\frac{dh}{dt} = 0 \tag{3.20}$$

$$\gamma = 0 \tag{3.21}$$

ii) Lower and upper bounds on the cruise speed:

$$0 \leq V \leq V_{max\ cruise} \tag{3.22}$$

3.2.9 Drag Model in Transition Phase

The net drag on the aircraft is assumed to be equivalent to the parasite drag on the fuselage and wings of the aircraft. Therefore, the net drag on the aircraft is calculated as follows [Yomchinda et al. (2011); DeMoss (2007); Pradeep and Wei (2018a); Pradeep et al. (2018)]:

$$D = \rho V^2 S_{ref} \frac{(C_{D0})_{fuselage} + C_D \sin\alpha}{2} \tag{3.23}$$

where $C_D = 1$ [Yomchinda et al. (2011)] and $S_{ref} \sin\alpha$ is the instantaneous equivalent flat plate area of the wings (combined) during the rotation of wings (transition phase).

3.2.10 Power Consumption in Transition Phase

The equation governing the power consumption by DEP of the tandem tilt-wing eVTOL aircraft in transition phase i.e. deceleration and hover (assuming DEP produce vertically upward thrust) is calculated as follows:

$$P = \frac{T v_h}{\eta_{prop}} \tag{3.24}$$

where T is the net thrust produced by DEP of the eVTOL, η_{prop} is the efficiency of the propeller and v_h is the induced velocity in hover.

Using momentum theory [Hoffmann et al. (2007); Johnson (2012)], the induced velocity (v_h) in hover is given by:

$$v_h = \sqrt{\frac{T_i}{2\rho A}} \tag{3.25}$$

where T_i is the thrust produced by the i^{th} rotor, A is the rotor disk area (πR^2), R is the radius of the rotor and ρ is the density of the air.

In this research, as stated earlier we have ignored mechanical energy losses during the rotation of wings and rotors from cruise to descent configuration. Therefore, the total energy consumed ($E_{transition}$) by DEP in transition phase is as follows:

$$E_{transition} = \int_0^{t_f^{transition}} P dt \tag{3.26}$$

3.2.11 Vertical Descent Flight Dynamics

Figure 3.4: Airbus Vahana: Tandem Tilt-Wing Configuration During the Descent Phase [Airbus-A^3 (2018)]

The equations of motion for the tandem tilt-wing eVTOL aircraft (shown in Figure 3.3) during the vertical descent are as follows [Johnson (2012, 1977); Bottasso et al. (2005); Yomchinda et al.

(2011)]:

$$\frac{dV}{dt} = \frac{W - T - D}{m} \tag{3.27}$$

$$\frac{dh}{dt} = V \tag{3.28}$$

$$T = \sum_{i=1}^{8} T_i \tag{3.29}$$

where h is the altitude of the center of mass, T is the net thrust, D is the parasite drag, T_i is the thrust produced by the i^{th} rotor, m is the mass, V is the true airspeed, W is the weight of the eVTOL aircraft and g is the acceleration due to gravity.

3.2.12 Path Constraint in Descent

In order to avoid Vortex Ring State (VRS) during the descent phase, the following additional path constraint is imposed on the descent phase of the problem [Chenglong et al. (2015); Pradeep and Wei (2018a); Pradeep et al. (2018)]:

$$-0.28 \leq \frac{V}{v_h} \leq 0 \tag{3.30}$$

where v_h is the induced velocity in hover.

3.2.13 Drag Model in Descent

The net drag on the aircraft is assumed to be equivalent to the parasite drag on the fuselage of the aircraft. Therefore, the net drag on the aircraft is calculated as follows [Yomchinda et al. (2011); DeMoss (2007)]:

$$D = \frac{\rho V^2 C_D F_{top}}{2} \tag{3.31}$$

where F_{top} is the equivalent top flat plate area of the fuselage and $C_D = 1$ [Yomchinda et al. (2011)].

3.2.14 Power Consumption in Descent

Consider a rotor in vertical descent at true airspeed V, the solution for induced velocity (v_i) is [Hoffmann et al. (2007); Johnson (2012)]:

$$v_i = \frac{v_h^2}{(-V + v_i)} \tag{3.32}$$

The power consumed by DEP in descent phase is as follows [Hoffmann et al. (2007); Johnson (2012)]:

$$P = \frac{T(-V + v_i)}{\eta_{prop}} \tag{3.33}$$

where T is the net thrust produced by the eVTOL.

Hence, the total energy consumed by DEP during the vertical descent is given by:

$$E_{descent} = \int_0^{t_f^{descent}} P dt \tag{3.34}$$

3.2.15 Phase link

Each of the three phases in the trajectory is linked to the adjoining phases by a set of linkage conditions [Rao et al. (2010)]. These constraints force the position (along-track and altitude) and velocity (horizontal component and vertical component) to be continuous [Pradeep and Wei (2018a); Pradeep et al. (2018)]. Hence, the problem is subject to phase link constraints on state variables (X) as follows [Rao et al. (2010)]:

$$X^{phase-1}(t_f^{phase-1}) = X^{phase}(t_0^{phase}) \tag{3.35}$$

3.2.16 Performance Index

The performance index (Lagrange type) of the multiphase optimal control problem for the vertical trajectory optimization of the eVTOL aircraft is as follows [Pradeep and Wei (2018a); Pradeep et al. (2018)]:

$$J = \sum_{N=1}^{3} \int_{t_0^N}^{t_f^N} (\sum_{i=1}^{8} P_i) dt \tag{3.36}$$

where i is the i^{th} rotor, P_i is the power consumption by the i^{th} rotor, and N is the vertical flight phase ($N = 1$ for cruise, $N = 2$ for transition and $N = 3$ for descent (arrival)).

3.3 Numerical Study

The equations of motion of the tandem tilt-wing eVTOL are continuous-time nonlinear differential equations [Pradeep and Wei (2018a); Pradeep et al. (2018)]. Therefore, a numerical-optimization technique (direct method) has been used in this research to solve the trajectory optimization problem.

GPOPS-II is a commercially available general-purpose MATLAB software for solving multi-phase optimal control problems using variable-order Gaussian quadrature collocation methods. The software employs a Legendre-Gauss-Radau quadrature orthogonal collocation (Pseudospectral) method where the continuous-time optimal control problem is transcribed to a large sparse nonlinear programming problem (NLP) [Rao et al. (2010)]. GPOPS-II has been used for direct transcription of the multiphase optimal control problem (minimum energy path). The IPOPT has been used as the solver to solve the problem transcribed to NLP by GPOPS-II [Wächter and Biegler (2006)]. The numerical simulation was performed on a MacBook Pro with 2.8 GHz Intel Core i7 Processor.

The initial condition (IC) and final condition (FC) for the multiphase optimal control problems are as shown in Table 3.2, Table 3.3 and Table 3.4.

Table 3.2: Initial and Final Conditions in Cruise

State Variable	**IC**	**FC**
Altitude	500 m	500 m
Along-track distance	0 m	Free

Table 3.3: Initial and Final Conditions in Transition

State Variable	**IC**	**FC**
Altitude	500 m	500 m
Along-track distance	Free	50000 m

Table 3.4: Initial and Final Conditions in Descent

State Variable	IC	FC
Altitude	500 m	5 m
Along-track distance	50000 m	50000 m

3.3.1 Results of Minimum Energy Trajectory for Various Constant Cruise Speed Missions with RTA Constraint (1500 Sec)

The energy consumption (Megajoule (MJ)), ground speed profiles (m/s) and flight time distributions (sec) for Airbus Vahana on various constant cruise speed missions (45.5, 50, 60, 70 and 80 m/s) with RTA constraint (1500 sec) are shown in Figure 3.5, Figure 3.6 and Figure 3.7. From the figures, it can be seen that while the tandem-tilt eVTOL aircraft is airborne; the delay absorption is most energy efficiently managed between cruise and hover by distributing the maximum possible delay to cruise phase followed by absorption of remaining delay in hover at the cruise altitude directly above the vertiport per the CONOP.

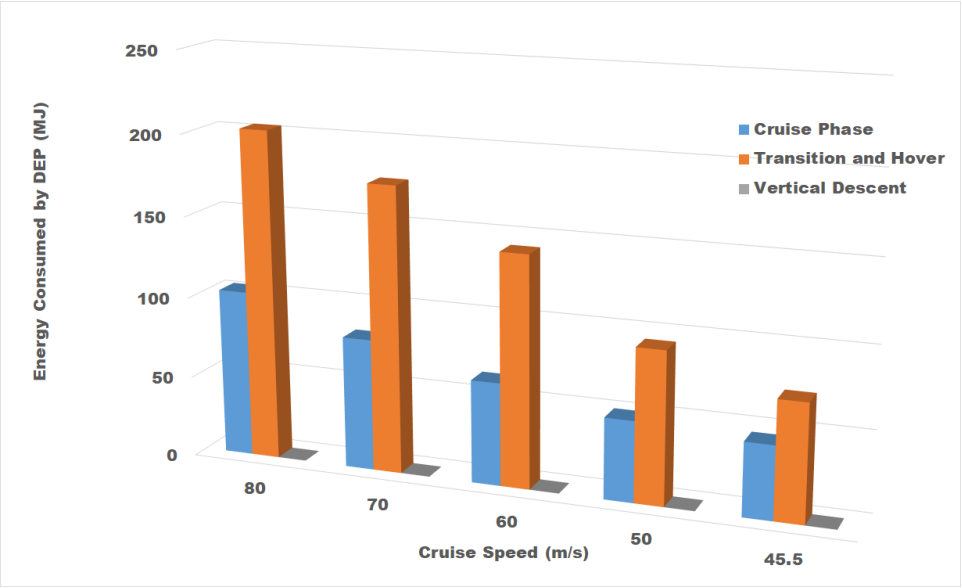

Figure 3.5: Energy Consumed by DEP for Various Cruise Speeds with Fixed RTA (1500 sec)

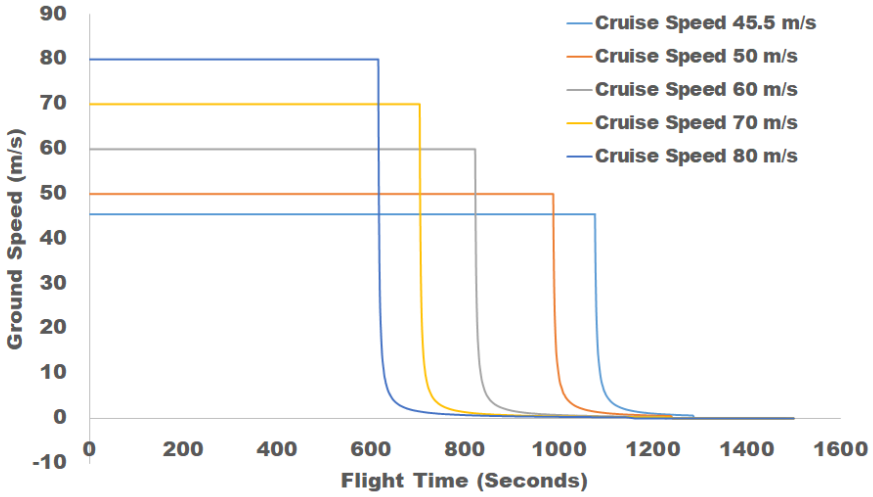

Figure 3.6: Ground Speed Profiles for Various Cruise Speeds with Fixed RTA (1500 sec)

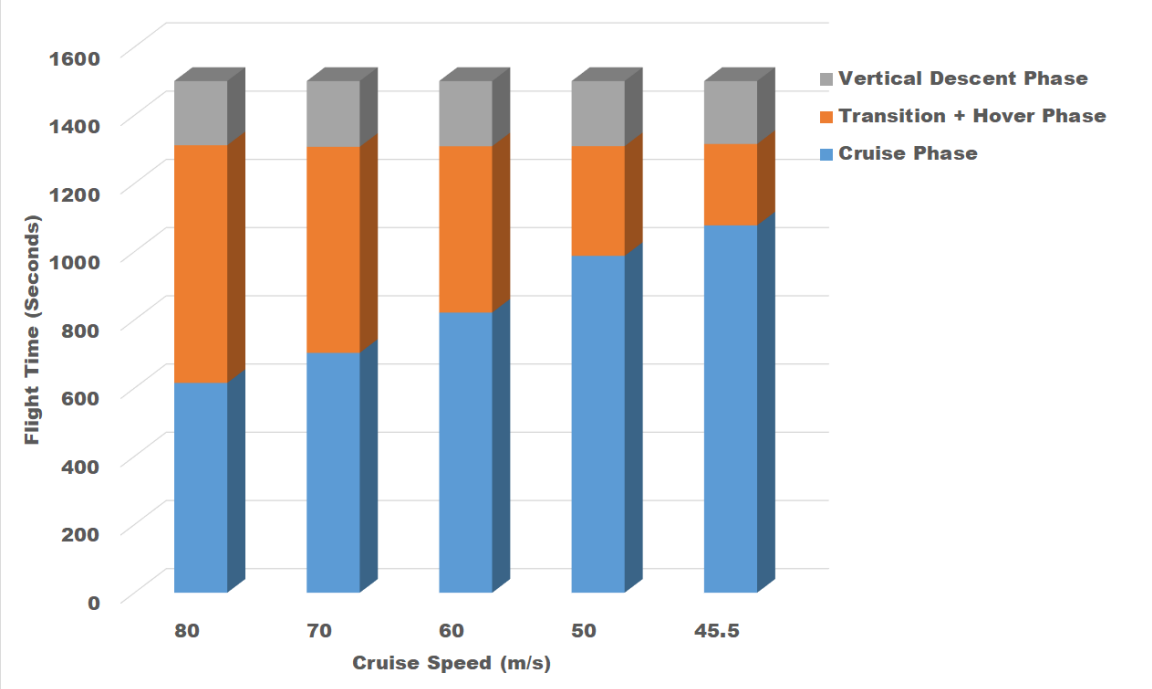

Figure 3.7: Flight Time Distribution for Various Cruise Speeds with Fixed RTA (1500 sec)

3.4 Conclusion

In this chapter of the dissertation, a multiphase optimal control problem with energy consumption as the performance index is formulated for a tandem-tilt eVTOL aircraft on urban air mobility (UAM) passenger transportation mission. Further, we present an optimal control framework to perform energy efficient arrival for a tandem-tilt urban eVTOL aircraft given the required time of arrival (RTA) constraint. The formulated vertical trajectory optimization problem is numerically solved using pseudospectral method for a specific eVTOL aircraft, i.e., Airbus Vahana. For the given CONOP of Airbus Vahana, the computational results show that while the tandem-tilt eVTOL aircraft is airborne; the delay absorption is most energy efficiently managed between cruise and hover by distributing the maximum possible delay to cruise phase followed by absorption of the remaining delay in hover at the cruise altitude directly above the vertiport.

CHAPTER 4. VALIDATION OF MULTIPHASE OPTIMAL CONTROL MODEL

4.1 Introduction

In this chapter of the dissertation, validation of the multiphase optimal control model is performed using a commercial quadrotor DJI Phantom 4.0. We used DJI Phantom 4.0 for the validation because of its known performance characteristics to the remote pilots and public.

4.2 Validation Using Numerical Method

As seen in chapter 2, the equations of motion of multirotor UAVs are continuous-time nonlinear differential equations and hence they are difficult to solve analytically. For this reason numerical-optimization technique has been used for validation of the multiphase optimal control model.

GPOPS-II has been used for validation of the multiphase optimal control problem. The IPOPT has been used as the solver to solve the problems transcribed to NLP by GPOPS-II [Wächter and Biegler (2006)]. The numerical simulation was performed on a Macbook Pro with 2.8 GHz Intel Core i7 Processor.

4.2.1 DJI Phantom 4.0

The path constraints imposed on DJI phantom 4.0 are as follows [Pradeep et al. (2018)]:

$$V_h^{climb} \leq 6\ m/s \tag{4.1}$$

$$-4\ m/s \leq V_h^{descent} \tag{4.2}$$

$$V_x^{phase} \leq 20\ m/s \tag{4.3}$$

$$h^{phase} \leq 121.92\ m\ (400\ ft) \tag{4.4}$$

$$-0.28 \leq (\frac{\sqrt{V_x^2 + V_h^2}\sin\alpha}{v_h})^{descent} \leq 0 \tag{4.5}$$

where state and control variables are the same as defined in the problem formulation section in chapter 2 of the dissertation.

The initial condition (IC) and final condition (FC) for the multiphase optimal control problems are as shown in Table 4.1. The performance data required to compute Thrust and Drag are as shown in Table 4.2.

Table 4.1: Initial and Final Conditions for Validation

State Variable	**IC**	**FC**
Altitude	5 m	5 m
Along-track distance	0 m	Free
Ground Speed (GS)	0.1 m/s	0.1 m/s
Time	0 s	1200 s

Table 4.2: Performance Data of DJI Phantom 4.0

Variable	**Value**
Rotor Diameter	0.24 m
Mass	1.410 Kg
Equivalent Front Plate Area	0.012 m^2
Equivalent Top Plate Area	0.03 m^2

4.2.2 Results of Minimum Energy Profiles for Various Constant Cruise Ground Speed Missions

The validation results of the fixed duration (20 mins) multiphase (climb, cruise and descent) optimal control problems are discussed in this section.

Finally, energy consumed (Kilo Joule (KJ)) by DJI Phantom 4.0 is plotted against various constant cruise ground speed missions, where each mission is of a fixed flight duration i.e. 20 mins.

The energy optimal vertical profiles and ground speeds for DJI Phantom 4.0 on various constant cruise ground speed missions (1, 3, 5, 7.5, 10, 12.5 and 15 m/s) are shown in Figure 4.1 and Figure 4.2. The numerical format of results from Figure 4.1 and Figure 4.2 are as shown in Table 4.3. From, Figure 4.1, Figure 4.2 and Table 4.3, it can be seen that higher the cruise ground speed greater is the corresponding range.

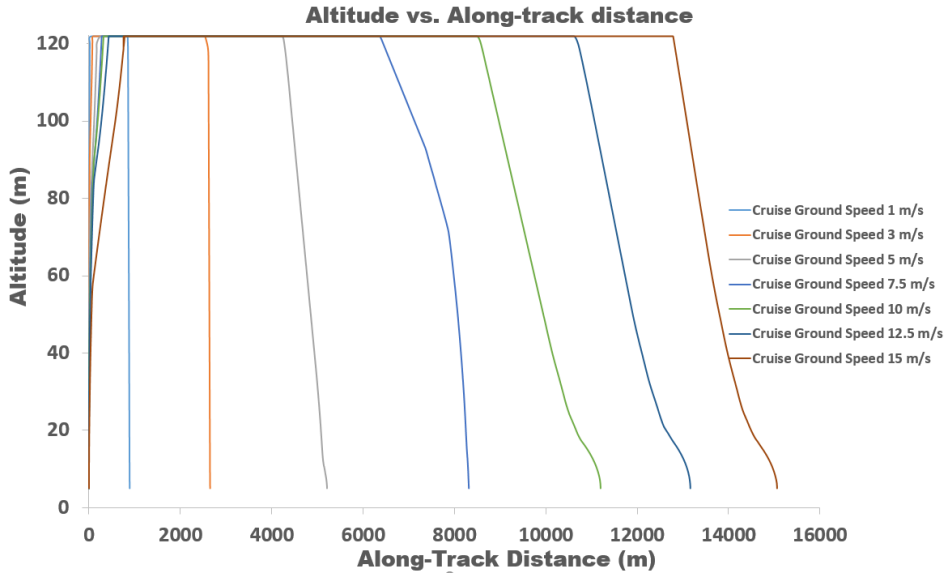

Figure 4.1: Minimum Energy: Vertical Profiles of DJI Phantom 4.0.

Table 4.3: Minimum Energy Cruise Ground Speed Vs. Range

Cruise Ground Speed (m/s)	**Range (m)**
1	892
3	2652
5	5210
7.5	8315
10	11198
12.5	13163
15	15061

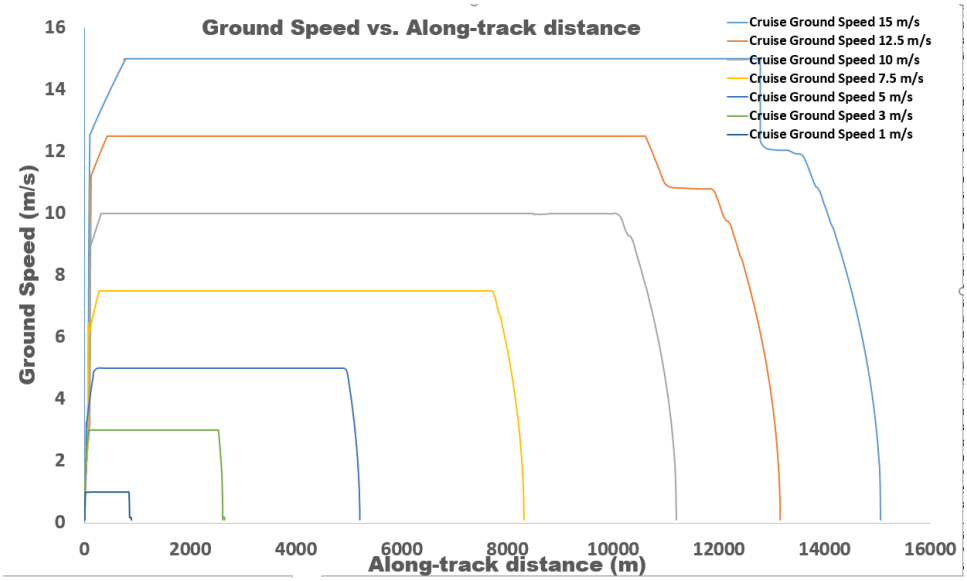

Figure 4.2: Minimum Energy: Ground Speed Profiles of DJI Phantom 4.0.

4.2.3 Minimum Energy Speed

The energy consumption (performance index) is calculated based on summation of induced power and parasite power, which is integrated over the total flight duration (20 mins). As stated before, the fixed duration (20 mins) flight with various constant cruise ground speeds (1, 3, 5, 7.5, 10, 12.5, 15 and 20 m/s) includes climb, cruise and descent phases. Based on the 3rd order polynomial fit of Figure 4.3 and the matlab function fminbnd, it is concluded that among the various constant cruise ground speed missions with a fixed flight duration (20 mins), the one with cruise ground speed of 12.089 m/s has the (global) minimum energy consumption.

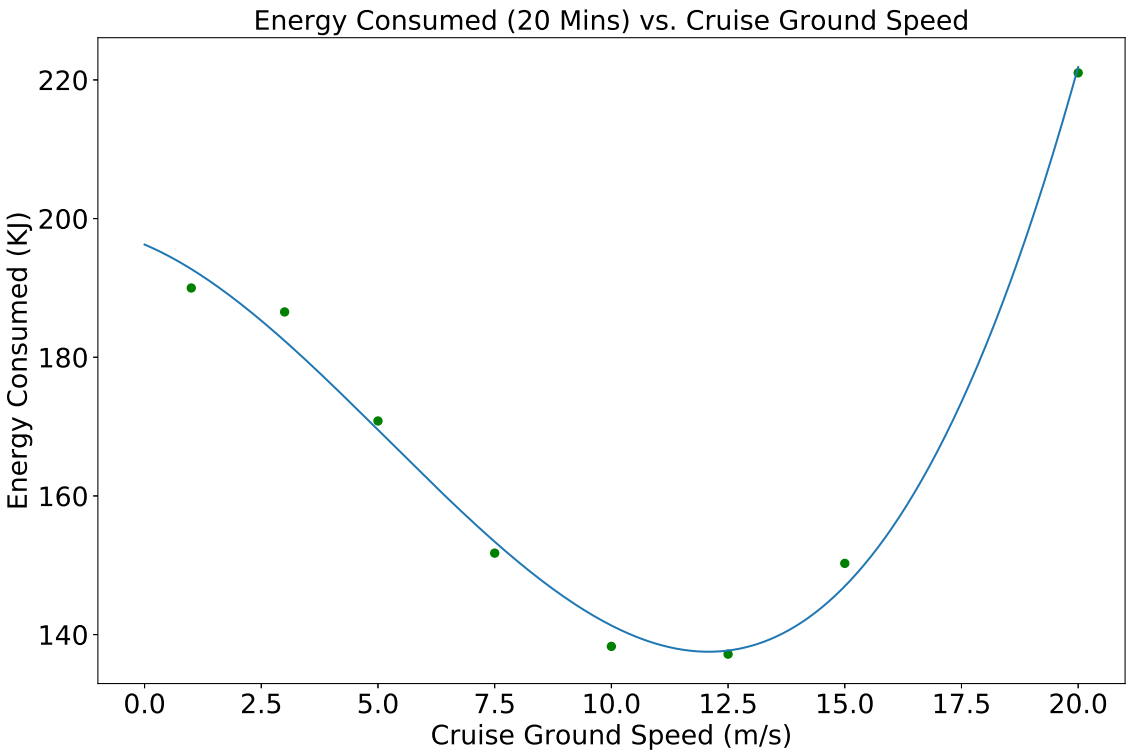

Figure 4.3: Energy Consumption vs. Cruise Ground Speed in 20 Minutes Flight

4.3 Conclusion

The minimum energy speed (12.089 m/s) computed for DJI Phantom 4.0 in this chapter of the dissertation is close to (less than 20 % off) return to home (RTH) speed (10 m/s) [Reid (2018)] of DJI Phantom 4.0. Therefore, the results in this chapter of the dissertation validates the optimal control model.

CHAPTER 5. ARRIVAL SEQUENCING AND SCHEDULING OF MIXED FLEET OF EVTOLS IN UAM

5.1 Introduction

In this chapter of the dissertation, arrival sequencing and scheduling problem for emergent and early expanded UAM operations for a mixed fleet of eVTOLs expected to land on a vertiport is presented.

5.2 Problem Statements for Emergent and Early Expanded UAM Operations

In this research, the ground infrastructure of the vertiport is assumed to be as follows: i) takeoff pads are separated from landing pads; ii) departure operations are independent of arrival operations; and iii) the ratio of the number of gates and staging stands to the number of landing pads (N) is optimal to support immediate taxi-in of an eVTOL aircraft to a gate or staging stand after the touchdown on the landing pad [Vascik and Hansman (2019)]. The descent is assumed to be vertical descent for both emergent (low traffic density) and early expanded (moderate/high traffic density) UAM operations. DEP powered eVTOLs have a higher downwash velocity compared to conventional helicopters that permits a more rapid vertical descent without entering a vortex ring state [Schrank et al. (2015)]. Therefore, eVTOLs are better suited for vertical descent than conventional helicopters. Moreover, the vertical descent would be exceptionally safe when skyscrapers surround the vertiport.

5.2.1 CONOPs for eVTOL Aircraft Arrival in Emergent UAM Operations

For emergent UAM operations [Thipphavong et al. (2018)] (low traffic density), the arrival concept of operations (CONOPs) for the mixed fleet of eVTOL aircraft (wingless/winged) is assumed to be cruising at a constant altitude followed by the vertical descent to land on the vertiport with

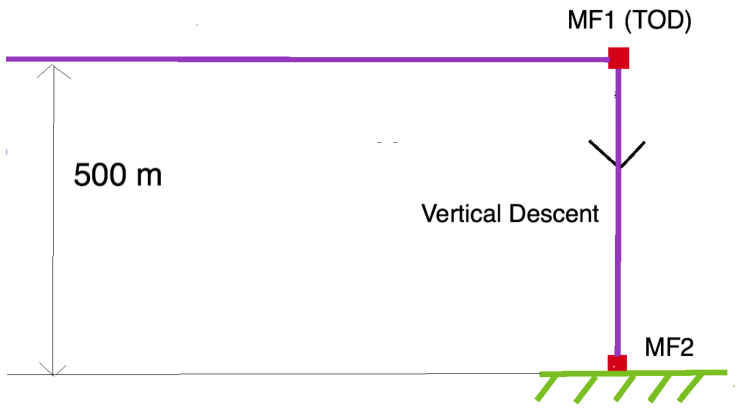

Figure 5.1: Vertical View of eVTOL Aircraft Arrival and Top View of Vertiport with Single Landing Pad [Airbus-A^3 (2018); Schrank et al. (2015)]

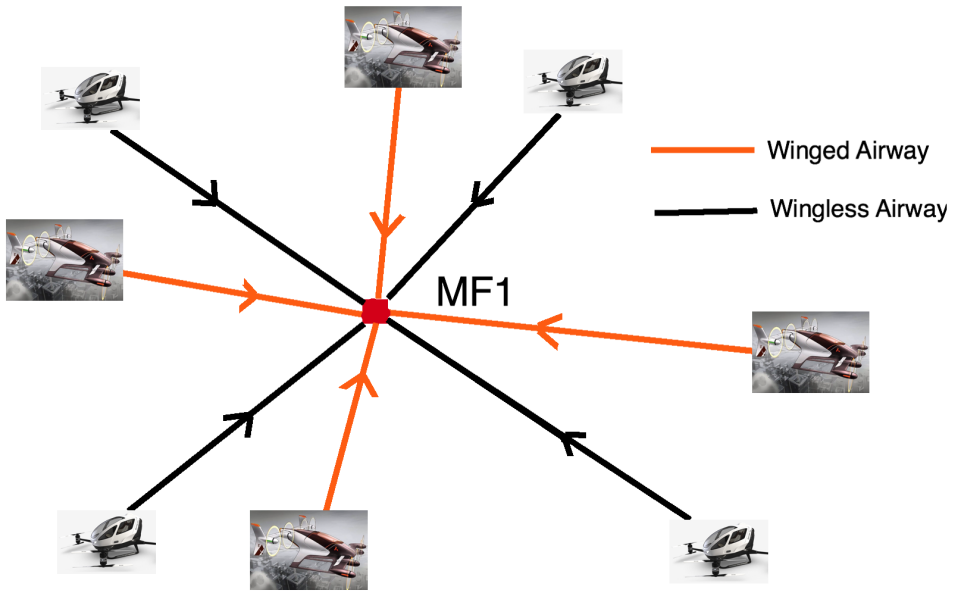

Figure 5.2: Lateral View of UAM Arrival Airspace in Low Traffic Density Flow

single landing pad. For low traffic density CONOP, we assumed the first metering fix (MF1) for arrival at cruise altitude directly above the vertiport and the second metering fix (MF2) at the vertiport itself.

The arrival routes (airways) for winged eVTOL are separated from the arrival routes (airways) of wingless eVTOLs because of difference in cruise speeds of winged and wingless eVTOLs [Airbus-A^3 (2018); EHang-184 (2018); Volocopter (2018)]. Therefore, we propose an airspace design concept to separate wingless eVTOL arrival air traffic from winged until merging at the metering fix as shown in Figure 5.2.

The ETA for each eVTOL aircraft to the MF1 is assumed to be based on the following: i) nominal cruise speed of the eVTOL aircraft, ii) airways to the first metering fix are geodesic path, iii) negligible time to decelerate to hover, and iv) no miles-in-trail enroute restrictions on the airways. The ETA for the i^{th} eVTOL aircraft to the MF2 is given by:

$$ETA(i)_{MF2} = ETA(i)_{MF1} + t_v(i) \quad \forall\ i \tag{5.1}$$

where $t_v(i)$ is the vertical time of descent for the i^{th} eVTOL aircraft. Since the MF1 is also a merging point for eVTOL air traffic in UAM, therefore, the ETAs of eVTOL aircraft to the MF1 is used to define the FCFS order.

5.2.2 CONOPs for eVTOL Aircraft Arrival in Early Expanded UAM Operations

For early expanded UAM operations [Thipphavong et al. (2018)] (moderate/high traffic density), the arrival concept of operations (CONOPs) for the mixed fleet of eVTOL aircraft (wingless/winged) is assumed to be cruising at a constant altitude followed by the descent (from fixed TOD) to land on the vertiport with single or multiple landing pads [Vascik and Hansman (2019)]. Similar to the low traffic density UAM operations, the arrival routes (airways) for winged eVTOLs are separated from the arrival routes (airways) of wingless eVTOLs because of difference in cruise speeds of winged and wingless eVTOLs [Airbus-A^3 (2018); EHang-184 (2018); Volocopter (2018)]. However, we propose an airspace design concept to merge wingless and winged eVTOL aircraft ar-

rival traffic at a metering gate (MG) as shown in Figure 5.3 and Figure 5.4. The waypoints located at the boundary of the terminal area of radius 400 m surrounding the vertiport as shown in Figure 5.3 and Figure 5.4 are referred to as metering gates [Erzberger and Itoh (2014); Kleinbekman et al. (2018)]. The metering gates are used as a means of controlling the UAM traffic flow rate into the vertiport during moderate and high traffic conditions [Erzberger and Itoh (2014); Kleinbekman et al. (2018)]. We assumed 400 m radius for the terminal region because it is sufficient to allow both winged and wingless to slow down from nominal cruise speed to hover with deceleration less than g/3.

In this research, for early expanded UAM operations, we assumed the first metering fix (MF1) for arrival at cruise altitude directly above the centroid of the topology of landing pads and the second metering fix (MF2) at the centroid itself. Given the safety requirement of minimum horizontal spacing of 200 ft between the centerline of landing pads (even for simultaneous descent operations of helicopters) [Vascik and Hansman (2019)], the descent from the MF1 (TOD) to any of the landing pads is assumed to be a vertical descent.

As stated, the location of MF1 (TOD) is assumed to be as defined in Table 5.1 and shown in Figure 5.3 and Figure 5.4 for a vertiport with different number of landing pads (N).

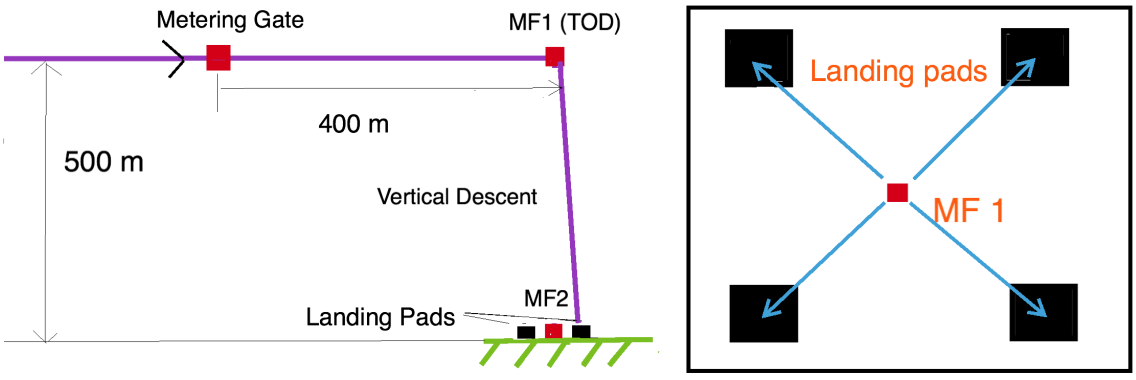

Figure 5.3: Vertical View of eVTOL Aircraft Arrival and Top View of Vertiport with Four Landing Pads

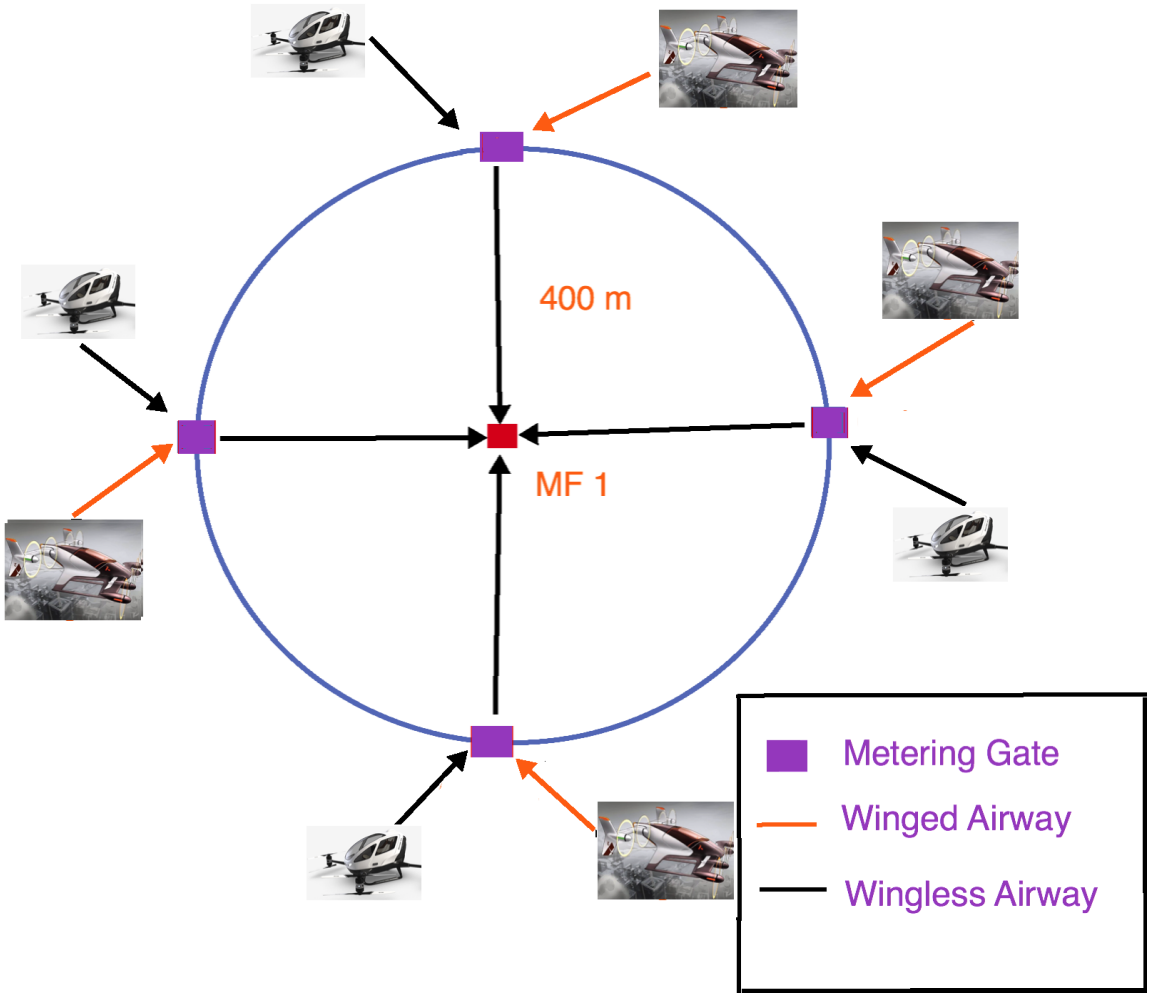

Figure 5.4: Lateral View of UAM Arrival Airspace in High Traffic Density Flow

Table 5.1: Topology of Landing Pad(s) on a Vertiport

Number of Landing Pads (N)	**Topology**
1	Point (center of the landing pad)
2	Line (center of each landing pad is placed at the end point)
3	Equilateral triangle (center of each landing pad is placed at the vertex)
4	Square (center of each landing pad is placed at the vertex)
5	Regular pentagon (center of each landing pad is placed at the vertex)
6	Regular hexagon (center of each landing pad is placed at the vertex)

The ETA for each eVTOL aircraft to the MF1 is assumed to be based on the following: i) nominal cruise speed of the eVTOL aircraft until sequencing a metering gate (MG), ii) airways to the metering gates are geodesic path, iii) same transition time to travel from a metering gate to the MF1 for both types of eVTOLs even though winged eVTOLs travel faster than wingless eVTOLs but they have to undergo configuration change before the vertical descent [Uber-Elevate (2016); Pradeep and Wei (2018a,b); Airbus-A^3 (2018); Thipphavong et al. (2018)], and iv) no miles-in-trail enroute restrictions on the airways. The ETA for the i^{th} eVTOL aircraft to the MF1 is given by:

$$ETA(i)_{MF1} = ETA(i)_{MG} + t(i)_{transition} \quad \forall\ i \tag{5.2}$$

$$ETA(i)_{MF2} = ETA(i)_{MF1} + t_v(i) \quad \forall\ i \tag{5.3}$$

where $t(i)_{transition}$ is the transition time for the i^{th} eVTOL to travel from a metering gate (MG) to the MF1 while decelerating to hover at the MF1 and $t_v(i)$ is the vertical time of descent for the i^{th} eVTOL aircraft. Since the boundary of terminal area is also a merging point for early expanded UAM air traffic, therefore, the ETAs of eVTOL aircraft to a metering gate is used to define the FCFS order.

5.2.3 Objective of the Arrival Sequencing and Scheduling Problem

The goal of a scheduler is to assign each aircraft in the arrival traffic a required time of arrival (RTA) to the metering fix. However, for safety the RTA(i) for the i^{th} eVTOL aircraft should lie between it's earliest time of arrival (E(i)) and latest time of arrival (L(i)) to the metering fix.

We anticipate that the arrival sequencing and scheduling service providers for eVTOL aircraft would like to land the sequence of eVTOLs as soon as possible, given the limitations with Li-Po batteries and safety concerns associated with air traffic congestion in the terminal area. The optimization problem of minimizing the makspan i.e. the RTA of the last eVTOL (in the mixed fleet) to the MF1 is equivalent to maximizing vertiport throughput [Malik and Jung (2016); Balakrishnan and Chandran (2006)]. Hence, the objective of this research is to find the eVTOL aircraft landing order heuristically for a given set of mixed fleet of eVTOLs such that the makespan of the eVTOLs

(n) expected to land is minimized. Therefore, the decision variables are the set of (RTA)s to the MF1 and the objective of the problem is to minimize the RTA of the last eVTOL aircraft to the MF1:

$$min.\ RTA(n)_{MF1} \tag{5.4}$$

5.2.4 Window Constraints on Arrival Scheduling

For both the operations (emergent and early expanded), the following window constraints are imposed on the $RTA(i)_{MF1}$ of each eVTOL aircraft, where i denotes the i^{th} aircraft in the arrival traffic sequence:

$$E(i)_{MF1} \leq RTA(i)_{MF1} \leq L(i)_{MF1} \quad \forall\ i \tag{5.5}$$

5.2.5 Minimum Time Separation in Emergent Operations

As emergent UAM operations is anticipated to involve low altitude operations [Schrank et al. (2015); Airbus-A^3 (2018); EHang-184 (2018); Thipphavong et al. (2018)] with low traffic density therefore we assumed vertiport with single landing pad. Therefore, we imposed a safety requirement that the trailing eVTOL aircraft shall not descend unless the leading has landed on the vertiport. Hence, the minimum time separation (Δt_{ij}) between the trailing eVTOL aircraft j and the leading eVTOL aircraft i is dependent on the vertical time of descent ($t_v(i)$) of the leading eVTOL aircraft (i) and is independent of the trailing eVTOL aircraft (j).

$$\Delta t_{ij} = t_v(i) \quad \forall\ i < j \tag{5.6}$$

Therefore, the following constraints have been imposed on the eVTOL sequencing and scheduling problem:

$$t_v(i) \leq RTA(j)_{MF1} - RTA(i)_{MF1} \quad \forall\ i < j \tag{5.7}$$

In this dissertation, the vertical descent is assumed to be from the cruise altitude of 500 m above sea-level to vertiport at sea-level. The vertical time of descent ($t_v(i)$) for winged and wingless eVTOLs is computed using the multiphase optimal control framework (minimum energy path)

from our previous research on trajectory optimization of Airbus Vahana and EHang 184 respectively [Pradeep and Wei (2018a,a)]. The multiphase optimal control problem is transcribed using GPOPS-II, and then IPOPT has been used as the solver to solve the problem transcribed to nonlinear programming by GPOPS-II [Rao et al. (2010); Wächter and Biegler (2006)].

Table 5.2: Minimum Time Separations (Sec) at the MF1

Leading eVTOLTrailing eVTOL	Winged	Wingless
Winged	151	151
Wingless	173	173

5.2.6 Minimum Time Separation in Early Expanded Operations

For early expanded operations (moderate/high traffic density), we imposed the minimum time separation (Δt_{ij}) between the trailing eVTOL aircraft j and the leading eVTOL aircraft i assuming dependency on the following: i) vertical time of descent ($t_v(i)$) of the leading eVTOL aircraft (i); ii) number of landing pads (N) on the vertiport; and iii) minimum temporal separation at the MF1; as shown in equation 5.8:

$$\Delta t_{ij} = max(45, \frac{t_v(i)}{N}) \quad \forall\ i < j \tag{5.8}$$

where $t_v(i)$ is as defined in Table 5.2.

Therefore, the following constraints have been imposed on the eVTOL sequencing and scheduling problem:

$$\Delta t_{ij} \leq RTA(j)_{MF1} - RTA(i)_{MF1} \quad \forall\ i < j \tag{5.9}$$

5.3 Proposed Algorithm

5.3.1 Insertion and Local Search Heuristics

The insertion and local search (ILS) heuristic algorithm developed in this dissertation for arrival sequencing and scheduling of eVTOL aircraft expected to land on a vertiport with single and

multiple landing pads, is based on the ILS algorithm described for single runway scheduling of commercial air traffic by Malik and Jung [Malik and Jung (2016)].

The heuristic starts with the initial guess for eVTOL aircraft arrival sequence as the FCFS to the MF1. The iteration begins for fixing the 1^{st} position in the arrival sequence and then it continues till fixing the $(n-k+1)^{th}$ position, where n is the total number of eVTOL aircraft expected to land on the vertiport and k is the number of free (moving window of free) eVTOL aircraft involved in each iteration for local neighborhood search (local optimization). For example, the i^{th} iteration for fixing the i^{th} position in the arrival sequence involves local neighborhood search starting from the i^{th} position in the sequence till the $(i+k-1)^{th}$ position. Hence, at each iteration $k!$ sequences (permutations) of eVTOL aircraft are possible. Therefore, local optimization is carried out $k!$ times to pick the preferred local sequence and fix the i^{th} position with the best eVTOL aircraft. During the local neighborhood search, the preferred sequence is the one with the least objective value among all the objective values in the $k!$ sequences. Hence, after the i^{th} iteration, the eVTOL aircraft positions from 1^{st} till i^{th} are considered fixed whereas the positions from $(i+1)^{th}$ till n^{th} are considered free. However, at the end of fixing the $(n-k+1)^{th}$ position, the eVTOL aircraft positions at $n+2-k, ..., n$ are fixed based on the preferred sequence for $(n-k+1)^{th}$ position in the arrival sequence as shown in Figure 5.5.

Consider a feasible sequence (H) consisting of n eVTOL aircraft $(a_1, a_2, a_3, ...a_n)$. For example, when $k = 3$, six different sequences (H_i^1, H_i^2, H_i^3, H_i^4, H_i^5, H_i^6) are possible during the i^{th} iteration by juggling eVTOL aircraft located at free neighborhood positions: $i, i+1$ and $i+2$ [Malik and Jung (2016)]. Figure 5.6, shows a few iteration steps of the ILS algorithm for $k = 3$ and fleet of 10 eVTOL aircraft expected to land, starting with the FCFS order. The green highlight indicates the preferred sequence of k free eVTOL aircraft during the i^{th} iteration that fixes the eVTOL aircraft for the i^{th} position in the sequence. The preferred sequence is the one with the least optimal objective value among all the six possibilities during the local neighborhood search. Finally, the i^{th} position (blue box in Figure 5.6) in the arrival sequence is fixed using the eVTOL aircraft at the i^{th} position in the preferred sequence during the iteration.

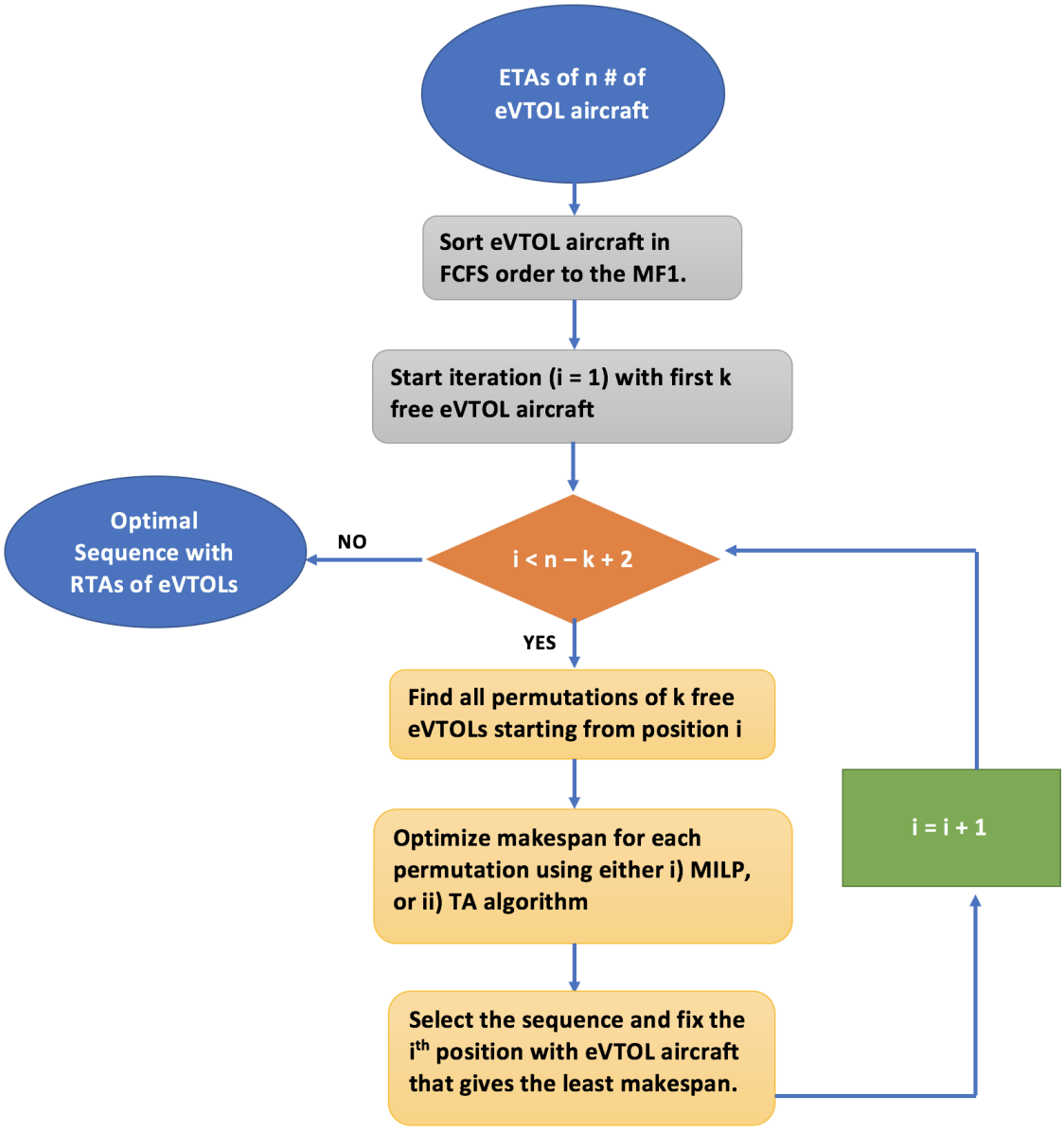

Figure 5.5: Block Diagram of Arrival Sequencing and Scheduling

As stated in the previous section, the objective function of the eVTOL aircraft arrival sequenc-

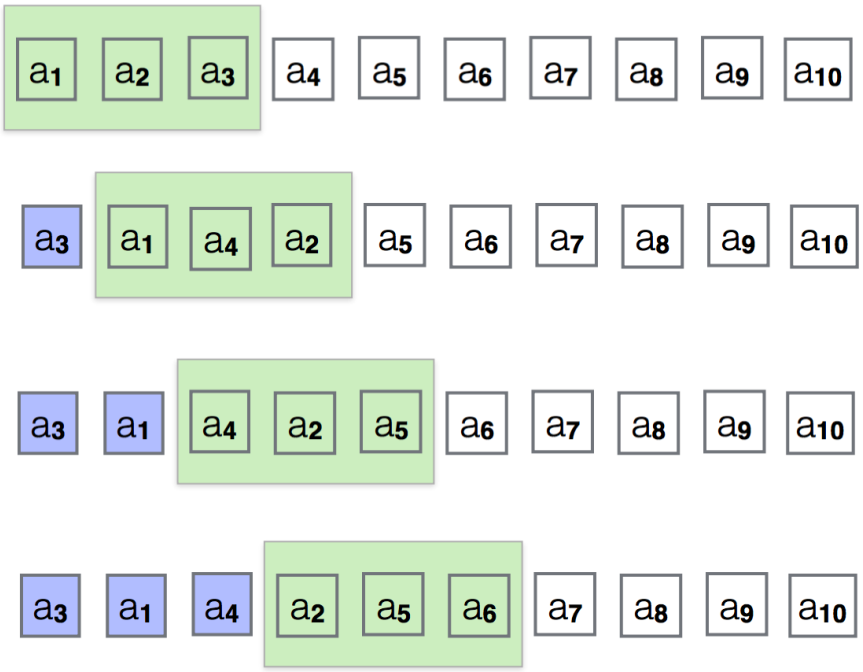

Figure 5.6: Example of ILS (k = 3) Algorithm for eVTOL Arrival Sequencing and Scheduling [Malik and Jung (2016)]

ing and scheduling problem is to minimize the RTA to the MF1 of the last eVTOL aircraft in the arrival sequence. The optimal objective value for each sequence in a given iteration is computed using either the open source MILP solver Gurobi Optimizer [Meindl and Templ ()] or in-house developed time advance (TA) algorithm [Neuman and Erzberger (1990); Balakrishnan and Chandran (2006)].

5.3.2 TA Algorithm

The main idea behind the TA algorithm is to speed-up an eVTOL whenever the separation from the leading eVTOL is larger than the minimum time separation (Δt_{ij}). Therefore, the $RTA(j)_{MF1}$ for the j^{th} eVTOL aircraft trailing behind the i^{th} eVTOL aircraft is given by:

$$RTA(j)_{MF1} = max\{E(j)_{MF1}, RTA(i)_{MF1} + \Delta t_{ij}\} \; \forall \; i < j \tag{5.10}$$

The above equation is based on the assumption that time to transition to hover is negligible. However, for the feasibility of the solution, the (RTA)s of all eVTOL aircraft to the MF1 should be less than their corresponding latest times of arrival to the MF1.

5.4 Numerical Simulations and Results

We anticipate arrival air traffic to a vertiport would be at random time distribution because of the on-demand nature of UAM but at an average rate when viewed as a group for a set of eVTOLs expected to land on a vertiport. Therefore, we simulated the estimated times of arrival (ETA)s of eVTOL aircraft using Poisson arrival process Willemain et al. (2004) using Python 3.6 (high-level programming language) [van Rossum and de Boer ()] on MacBook Pro with 2.8 GHz Intel Core i7 processor. In this research, irrespective of air traffic density (emergent or early expanded) we simulated two types of eVTOL air traffic, i.e., winged and wingless, both arriving via different airways and merging at the MF1 or MG depending upon arrival procedure (traffic density).

The winged eVTOL aircraft in the air traffic are simulated per the performance characteristics

Table 5.3: Performance Data of eVTOL Aircraft

eVTOL Type	**Nominal Cruise Speed** (m/s)	**VMO** (m/s)
Winged	45.5	80
Wingless	27.77	33.33

of Airbus Vahana [Airbus-A^3 (2018); Pradeep and Wei (2018b)] whereas wingless eVTOL aircraft are simulated per the performance characteristics of EHang 184 [EHang-184 (2018); Pradeep and Wei (2018a)] as shown in Table 5.3.

5.4.1 Numerical Simulations for Emergent Operations

For emergent operations (low traffic density), the earliest time of arrival of each eVTOL to the MF1 is calculated by ignoring transition and hover time. Therefore, the earliest time of arrival $(E(i))$ of the i^{th} eVTOL aircraft to the MF1 is calculated based on the maximum speed of the

eVTOL aircraft as follows:

$$E(i)_{MF1} = \frac{V_{cruise}}{VMO} * ETA(i)_{MF1} \quad \forall\ i \tag{5.11}$$

where V_{cruise} is the nominal cruise speed and VMO is the maximum cruise speed of the eVTOL aircraft.

The latest time of arrival ($L(i)$) of the i^{th} eVTOL aircraft to the MF1 should be ideally calculated based on the CONOP and state-of-charge (SOC) of the Li-Po battery pack of the eVTOL aircraft [Kulkarni et al. (2018); Bole et al. (2014)]. However, in the current research it is set as follows because of unavailability of battery model for EHang 184 and Airbus Vahana:

$$L(i)_{MF1} = ETA(i)_{MF1} + U(t) \quad \forall\ i \tag{5.12}$$

where $U(t)$ is a random function which uniformly samples a value between 900 and 1200 seconds. In this dissertation, we used function $U(t)$ to simulate the effect of CONOP and SOC of the Li-Po battery pack on the ETA of an eVTOL.

5.4.2 Numerical Simulations for Early Expanded Operations

For early expanded operations (moderate/high traffic density), the earliest time of arrival of each eVTOL to the boundary of terminal area (a metering gate) of the vertiport is calculated by assuming maximum cruise speed of the eVTOL. Therefore, the earliest time of arrival ($E(i)$) of the i^{th} eVTOL aircraft to a MG is as follows:

$$E(i)_{MG} = \frac{V_{cruise}}{VMO} * ETA(i)_{MG} \quad \forall\ i \tag{5.13}$$

where V_{cruise} is the nominal cruise speed and VMO is the maximum cruise speed of the eVTOL aircraft.

The earliest time of arrival ($E(i)$) of the i^{th} eVTOL aircraft to the MF1 is as follows:

$$E(i)_{MF1} = E(i)_{MG} + t_{transition} \tag{5.14}$$

In this dissertation, the transition time ($t_{transition}$) is assumed to be 30 seconds for both the eVTOL types. The assumption is based on passenger comfort, therefore, limiting the absolute value of deceleration in the terminal area to less than g/3 (where g is the acceleration due to gravity).

The latest time of arrival ($L(i)$) of the i^{th} eVTOL aircraft to to the boundary of terminal area (a MG) should be ideally calculated based on the CONOP and state-of-charge (SOC) of the Li-Po battery pack of the eVTOL aircraft [Kulkarni et al. (2018); Alnaqeb et al. (2018)]. However, in the current research it is set as follows because of unavailability of battery model for EHang 184 and Airbus Vahana:

$$L(i)_{MG} = ETA(i)_{MG} + U(t) \quad \forall\ i \tag{5.15}$$

where $U(t)$ is a random function which uniformly samples a value between 900 and 1200 seconds. In this dissertation, we used function $U(t)$ to simulate the effect of CONOP and SOC of the Li-Po battery pack on the ETA of an eVTOL.

The latest time of arrival ($L(i)$) of the i^{th} eVTOL aircraft to the MF1 is assumed as follows:

$$L(i)_{MF1} = L(i)_{MG} + t_{transition} \tag{5.16}$$

5.4.3 Results of Emergent Operations

The proposed heuristic methods (ILS-MILP and ILS-TA) to minimize the makespan of a given set of eVTOLs are written in Python 3.6 and run on MacBook Pro with 2.8 GHz Intel Core i7 processor. In this research, for emergent operations, we assumed mixed fleet of 10 eVTOL aircraft expected to land in 1800 seconds on a vertiport with single landing pad. The algorithms are tested using the case studies as described in this section.

5.4.3.1 Case study I - fleet mix ratio (5/5)

In this case study, the ETAs of 5 winged and 5 wingless eVTOL aircraft are generated separately using Poisson arrival process assuming a total time interval of 1800 seconds for each fleet.

From Table 5.4, we can observe that for the simulated mixed fleet of eVTOLs and their respective (ETA)s to the MF1, both the methods (ILS-MILP and ILS- TA) minimized the makespan

(RTA of the last eVTOL to the MF1) to the same value (1517.68 seconds). The minimization of the makespan was achieved by speeding-up eVTOLs whenever possible without violating any constraints. Also, it can be seen that for this simulation the preferred landing order (sequence) is FCFS. However, ILS-MILP method computed the optimal landing order and RTAs in 0.729 seconds whereas ILS-TA method computed the optimal results in 0.012 seconds.

5.4.3.2 Case study II - fleet mix ratio (7/3)

In this case study, the ETAs of 7 winged and 3 wingless eVTOL aircraft are generated separately using Poisson arrival process assuming a total time interval of 1800 seconds for each fleet.

From Table 5.5, we can observe that for the simulated mixed fleet of eVTOLs and their respective (ETA)s, both the methods (ILS-MILP and ILS-TA) minimized the makespan (RTA of the last eVTOL to the MF1) to the same value (1604.48 seconds) by changing the landing order and by speeding-up eVTOLs whenever possible without violating any constraints. The multiple shuffles in landing order show landing priority given to winged eVTOLs compared to wingless eVTOLs for minimization of the makespan because of the faster cruise speed of the former. For example, the initial landing order (6) of the wingless eVTOL is changed to 9 after the optimization. Again, ILS-MILP method computed the optimal landing order and (RTA)s in more time (0.702 seconds) compared to ILS-TA method (0.013 seconds).

5.4.3.3 Case study III - fleet mix ratio (3/7)

From Table 5.6, we can observe that for the simulated mixed fleet of eVTOLs and their respective (RTA)s, both the methods (ILS-MILP and ILS-TA) minimized the makespan (RTA of the last eVTOL to the MF1) to the same value (1735.43 seconds) by changing the landing order and by speeding-up eVTOLs whenever possible without violating any constraints. The shuffle in landing order 8 and 9 reiterates the point that overtaking and speeding-up of winged eVTOLs is one of the key factors in minimization of the makespan. Again, the computational time (0.743 seconds) of ILS-MILP method is higher than computational time (0.014 seconds) of ILS-TA method.

Table 5.4: Case Study I: Simulation of eVTOLs and Results of ILS-MILP and ILS-TA Methods

Simulations			**Results**			
FCFS	**eVTOL Type**	**ETA (Sec)**	**Sequence (MILP)**	**RTA (Sec)**	**Sequence (TA)**	**RTA (Sec)**
1	Winged	77.88	1	48.68	1	48.68
2	Wingless	82.82	2	199.68	2	199.68
3	Wingless	119.38	3	372.68	3	372.68
4	Wingless	157.40	4	545.68	4	545.68
5	Wingless	183.93	5	718.68	5	718.68
6	Wingless	245.64	6	891.68	6	891.68
7	Winged	1361.62	7	1064.68	7	1064.68
8	Winged	1493.70	8	1215.68	8	1215.68
9	Winged	1759.36	9	1366.68	9	1366.68
10	Winged	1820.91	10	1517.68	10	1517.68

Table 5.5: Case Study II: Simulation of eVTOLs and Results of ILS-MILP and ILS-TA Methods

Simulations			**Results**			
FCFS	**eVTOL Type**	**ETA (Sec)**	**Sequence (MILP)**	**RTA (Sec)**	**Sequence (TA)**	**RTA (Sec)**
1	Winged	100.31	1	62.69	1	62.69
2	Wingless	339.28	2	282.72	2	282.72
3	Winged	358.97	3	455.72	3	455.72
4	Wingless	657.59	4	606.72	4	606.72
5	Winged	1056.93	5	779.72	5	779.72
6	Wingless	1392.26	7	978.48	7	978.48
7	Winged	1565.58	8	1129.48	8	1129.48
8	Winged	1622.93	9	1280.48	9	1280.48
9	Winged	1685.24	6	1431.48	6	1431.48
10	Winged	1921.41	10	1604.48	10	1604.48

Table 5.6: Case Study III: Simulation of eVTOLs and Results of ILS-MILP and ILS-TA Methods

Simulations			**Results**			
FCFS	**eVTOL Type**	**ETA (Sec)**	**Sequence (MILP)**	**RTA (Sec)**	**Sequence (TA)**	**RTA (Sec)**
1	Wingless	148.90	1	124.08	1	124.08
2	Wingless	474.53	2	395.43	2	395.43
3	Wingless	539.73	3	568.43	3	568.43
4	Wingless	560.09	4	741.43	4	741.43
5	Winged	602.34	5	914.43	5	914.43
6	Wingless	767.72	6	1065.43	6	1065.43
7	Wingless	830.62	7	1238.43	7	1238.43
8	Wingless	960.75	9	1411.43	9	1411.43
9	Winged	1096.67	8	1562.43	8	1562.43
10	Winged	1674.03	10	1735.43	10	1735.43

5.4.4 Results of Early Expanded Operations

5.4.4.1 Case study IV - impact of number of landing pads (N) on makespan

In this research, for early expanded operations (moderate/high traffic density), we assumed mixed fleet of 80 eVTOL aircraft expected to land in 3600 seconds on a vertiport with single or multiple landing pads. In this case study, impact of number of landing pads (as defined in Table 5.1) on makespan (arrival throughput) is studied using the proposed ILS-TA heuristic method with k = 5. The original makespan of the simulated eVTOLs is 3383.21 seconds without imposing the minimum separation constraint between the eVTOLs at MF1. The minimum separation imposed between the eVTOLs using ILS-TA algorithm is per Table 5.2 and equation 5.8. Table 5.7 shows the impact of number of landing pads (N) on makespan (arrival throughput). From Table 5.7, it can be seen that with minimum time separation of 45 seconds the optimal result is achieved by using a vertiport with 4 landing pads per MF1 (TOD) for the proposed arrival procedure.

Table 5.7: Impact of Number of Landing Pad(s) on Makespan

Number of Landing Pads	**Makespan (ILS-TA) (Sec)**
1	12836.15
2	6442.65
3	4311.48
4	3604.15
5	3604.15
6	3604.15

5.4.5 Sensitivity Analysis

5.4.5.1 Case study VI - impact of moving window of free eVTOLs (k) on computational time and makespan

To study, the impact of moving window of free eVTOLs (k) involved in each local optimization (neighborhood search), on the computational time of the heuristic algorithm and makespan of the set of eVTOLs, the following UAM air-traffic have been simulated:

i) Emergent Operations: Eight eVTOLs (n) at Poisson arrival rate of 1 eVTOL per 180 seconds consisting of 4 winged and 4 wingless eVTOLs.

ii) Early Expanded Operations: Hundred eVTOLs (n) at Poisson arrival rate of 100 per hour consisting of 50 winged and 50 wingless eVTOLs.

The computational time of ILS-TA algorithm with a different number of moving window of free eVTOLs (k: 3, 4, 5, 6, 7, 8) involved in each local optimization (local neighborhood search) is calculated and compared for emergent operations as shown in Table 5.8. Similarly, the makespan of the emergent UAM air-traffic computed using ILS-TA algorithm with different k values is compared as shown in Table 5.8. The original makespan of the simulated eVTOLs is 908.92 seconds without imposing the minimum separation constraint between the eVTOLs. The minimum separation imposed between the eVTOLs using ILS-TA algorithm is per Table 5.2. Table 5.8 shows the impact of k on the: i) number of local searches per iteration, ii) makespan, and iii) overall computational time of the algorithm.

Table 5.8: Sensitivity Analysis of Moving Window of Free eVTOLs (k) for Emergent Operations

k	**Number of Local Searches**	**Makespan (ILS-TA) (Sec)**	**Computational Time (ILS-TA) (ms)**
3	6	1170.44	8.93
4	24	1170.44	49.95
5	120	1170.44	212.94
6	720	1170.44	960.66
7	5040	1170.44	6202.86
8	40320	1170.44	47020.0

The computational time of ILS-TA algorithm with a different number of moving window of free eVTOLs (k: 3, 4, 5, 6, 7) involved in each local optimization (neighborhood search) is calculated and compared for early expanded operations as shown in Table 5.9. Similarly, the makespan of the early expanded UAM air-traffic computed using ILS-TA algorithm with different k values is compared as shown in Table 5.9. The original makespan of the simulated eVTOLs is 3604.31 seconds without imposing the minimum separation constraint between the eVTOLs. The minimum separation imposed between the eVTOLs using ILS-TA algorithm is 30 seconds. Table 5.9 shows the impact of k on the: i) number of local searches per iteration, ii) makespan, and iii) overall computational time of the algorithm.

Table 5.9: Sensitivity Analysis of Moving Window of Free eVTOLs (k) for Early Expanded Operations

k	**Number of Local Searches**	**Makespan (ILS-TA) (Sec)**	**Computational Time (ILS-TA) (Sec)**
2	2	3203.18	0.71
3	6	3174.48	1.37
4	24	3168.59	7.98
5	120	3163.34	39.68
6	720	3162.34	211.24
7	5040	3162.34	1479.08

From Table 5.8 and Table 5.9, the following can be observed: i) For low density (emergent) operations with approximately 10 or fewer eVTOLs (arrival in half an hour) to be scheduled using the heuristic algorithm (ILS-TA) with k=3 produces an optimal result with computational time in milliseconds (8.93 ms); ii) For early expanded operations (moderate/high traffic density) with approximately 100 eVTOLs arrival scheduled to land in an hour, the heuristic algorithm (ILS-TA) with k=3 produces sub-optimal (near optimal) arrival sequencing and scheduling result, however with a considerably lower computational time (1.37 seconds) compared to computational times at higher values of k i.e. 6 and 7.

5.5 Conclusion

In this chapter of the dissertation, we formulated eVTOL aircraft sequencing and scheduling problem in urban air mobility (UAM) context for a mixed fleet (winged/wingless) of eVTOLs expected to land on a vertiport. Based on anticipated UAM traffic density in emergent (low) and early expanded (moderate/high) operations, two separate vertiport arrival procedures have been proposed for the problem. The arrival procedure for early expanded operations is proposed based on arrival procedure of emergent operations as a baseline with the addition of metering gate(s) on the boundary of the terminal area (a circular area of radius 400 m around a vertiport) and multiple landing pads on the vertiport. The objective of the problem is to minimize the makespan of a given set of eVTOLs, which is equivalent to maximizing the arrival throughput. The landing order (sequence) and makespan of the mixed fleet are determined using a heuristic approach called insertion and local search (ILS) combined with two different scheduling methods i) mixed-integer linear programming (MILP) or ii) time-advance (TA) algorithm. The optimization results show that for minimization of the makespan it is essential to i) speed-up a trailing eVTOL whenever separation from the leading is more than minimum separation, and ii) winged eVTOLs should have designated airways separate from wingless eVTOLs so that they can overtake earlier landing slot(s) of wingless eVTOLs whenever possible.

Upon applying ILS-TA algorithm on simulation of early expanded UAM operations the results showed the need for multiple landing pads in order to enable safe and efficient arrival. For minimum temporal separation of 45 seconds and proposed CONOP, a vertiport with 4 landing pads is the optimal configuration.

The sensitivity analysis using MacBook Pro with 2.8 GHz Intel Core i7 indicates the following:

(i) ILS-TA is computationally faster than ILS-MILP and produces the same optimal results. Also, it can be seen that ILS-TA algorithm can schedule 250 eVTOLs in less than 10 seconds.

(ii) For low density (emergent) operations with approximately 10 or fewer eVTOLs to be scheduled (arrival in half an hour) using the heuristic algorithm (ILS-TA) with k=3 produces an optimal result with computational time in milliseconds (8.93 ms). However, for early expanded operations (moderate/high traffic density) with approximately 100 eVTOLs arrival scheduled to land in an hour, the heuristic algorithm (ILS-TA) with k=3 produces sub-optimal (near optimal) arrival sequencing and scheduling result, however with a considerably lower computational time (1.37 seconds) compared to computational times at higher values of k i.e. 6 and 7.

CHAPTER 6. CONCLUSIONS AND FUTURE WORK

In this final chapter, all the work presented in this dissertation is summarized, and recommendations for future work are discussed.

6.1 Contributions

The contributions from the first part of the research are as follows:

- The longitudinal dynamics of a multirotor eVTOL have been decoupled from lateral dynamics to solve the vertical trajectory optimization problem as 2D flight dynamics problem in the vertical plane.
- The formulated vertical trajectory optimization problem is numerically solved using the pseudospectral method for a specific multirotor eVTOL aircraft, i.e., EHang 184 and five different types of CONOPs. The numerical results of the fixed pitch case study suggest that the collective pitch mechanism is required for the operational feasibility of a multirotor eVTOL aircraft like EHang 184 considering passenger comfort.
- By imposing various arrival time constraints on the eVTOL aircraft, observed that for the energy efficient arrival operations, the airborne delay is best absorbed by CONOP 5, i.e., the combination of cruise speed control and descent speed control with a shallow descent path to the meter fix. The airborne delay absorption by hovering (CONOP 4) at the cruise altitude is the least energy efficient of all.
- The numerical solutions showed that with an increase in flight duration there is an increase in the total energy consumption and therefore a clear need for higher stored energy in the onboard Li-Po batteries of the eVTOL aircraft.

- Similar to multirotor eVTOL, the longitudinal dynamics of a tandem tilt-wing eVTOL have been decoupled from lateral dynamics to solve the vertical trajectory optimization problem as 2D flight dynamics problem in the vertical plane.

- The formulated problem is numerically solved using pseudospectral method for a specific eVTOL aircraft, i.e., Airbus Vahana. For the CONOP proposed by Airbus Vahana group, the computational results show that while the tandem-tilt eVTOL aircraft is airborne; the delay absorption is most energy efficiently managed between cruise and hover by distributing the maximum possible delay to cruise phase followed by absorption of the remaining delay in hover at the cruise altitude directly above the vertiport.

- Finally, the optimal control problem formulation is validated using a commercial quadrotor DJI Phantom 4.0. DJI Phantom 4.0 has been used for the validation because of its known performance characteristics to the remote pilots and public.

The contributions from the second part of the research are as follows:

- The eVTOL aircraft sequencing and scheduling problem have been formulated in urban air mobility (UAM) context for a mixed fleet (winged/wingless) of eVTOLs expected to land on a vertiport.

- The objective of the problem is to minimize the makespan of a given set of eVTOLs, which is equivalent to maximizing the arrival throughput.

- Based on anticipated UAM traffic density in emergent (low) and early expanded (moderate/high) operations, two separate vertiport arrival procedures have been proposed for the problem. The arrival procedure for early expanded operations is proposed based on arrival procedure of emergent operations as a baseline with the addition of metering gate(s) on the boundary of the terminal area (a circular area of radius 400 m around a vertiport) and multiple landing pads on the vertiport.

- The landing order (sequence) and makespan of the mixed fleet are determined using a heuristic approach called insertion and local search (ILS) combined with two different scheduling methods i) mixed-integer linear programming (MILP) or ii) time-advance (TA) algorithm.
- The optimization results show that for minimization of the makespan it is essential to i) speed-up a trailing eVTOL whenever separation from the leading is more than minimum separation, and ii) winged eVTOLs should have designated airways separate from wingless eVTOLs so that they can overtake earlier landing slot(s) of wingless eVTOLs whenever possible.
- Upon applying ILS-TA algorithm on simulation of early expanded UAM operations, the results showed the need for multiple landing pads to enable safe and efficient arrival. For minimum temporal separation of 45 seconds and proposed CONOP, a vertiport with 4 landing pads is the optimal configuration.
- ILS-TA is computationally faster than ILS-MILP and produces the same optimal results.
- Using MacBook Pro with 2.8 GHz Intel Core i7, for low density (emergent) operations with approximately 10 or fewer eVTOLs (arrival in half an hour) to be scheduled using the heuristic algorithm (ILS-TA) with k=3 produces an optimal result with computational time in milliseconds (8.93 ms). However, for early expanded operations (moderate/high traffic density) with approximately 100 eVTOLs arrival scheduled to land in an hour, the heuristic algorithm (ILS-TA) with k=3 produces sub-optimal (near optimal) arrival sequencing and scheduling result, however with a considerably lower computational time (1.37 seconds) compared to computational times at higher values of k i.e. 6 and 7.

6.2 Future Research

The following are the primary future directions and possible extensions of the research presented in this dissertation:

- In the future, for a longer airborne delay absorption by an eVTOL in early expanded and matured UAM operational environment, priority and weightage of the combination of the

following three strategies: (i) cruise speed control, (ii) descent speed control and (iii) descent path modification, needs to be further investigated.

- For assessment of UAS/UAM flight mission completion using multiphase optimal control framework, research on the integration of the flight dynamics model, wind model, and battery prognostic model need to be performed.
- For arrival sequencing and scheduling problem in UAM, more arrival and approach procedures need to be investigated followed by sensitivity analysis.

BIBLIOGRAPHY

Airbus-A^3 (2018). Vahana aero. https://vahana.aero/. [Online; accessed 14-November-2018].

Alnaqeb, A. H., Li, Y., Lui, Y.-H., Pradeep, P., Wallin, J., Hu, C., Hu, S., and Wei, P. (2018). Online prediction of battery discharge and flight mission assessment for electrical rotorcraft. In *2018 AIAA Aerospace Sciences Meeting*, page 2005.

Altawy, R. and Youssef, A. M. (2016). Security, privacy, and safety aspects of civilian drones: A survey. *ACM Transactions on Cyber-Physical Systems*, 1(2):7.

Anagnostakis, I., Clarke, J.-P., Bohme, D., and Volckers, U. (2001). Runway operations planning and control sequencing and scheduling. In *Proceedings of the 34th Annual Hawaii International Conference on System Sciences*, pages 12–pp. IEEE.

Balakrishnan, H. and Chandran, B. (2006). Scheduling aircraft landings under constrained position shifting. In *AIAA guidance, navigation, and control conference and exhibit*, page 6320.

Balakrishnan, H. and Chandran, B. G. (2010). Algorithms for scheduling runway operations under constrained position shifting. *Operations Research*, 58(6):1650–1665.

Bole, B., Daigle, M., and Gorospe, G. (2014). Online prediction of battery discharge and estimation of parasitic loads for an electric aircraft. *ESC*, 2:5S2P.

Bosson, C. and Lauderdale, T. A. (2018). Simulation evaluations of an autonomous urban air mobility network management and separation service. In *2018 Aviation Technology, Integration, and Operations Conference*, page 3365.

Bottasso, C. L., Croce, A., Leonello, D., and Riviello, L. (2005). Rotorcraft trajectory optimization with realizability considerations. *Journal of Aerospace Engineering*, 18(3):146–155.

Bryson, A. E. (2018). *Applied optimal control: optimization, estimation and control*. Routledge.

Cao, Y., DeLaurentis, D., and Sun, D. (2013). Benefit and trade-off analysis of continuous descent approach in normal traffic conditions. *Transportation Research Record: Journal of the Transportation Research Board*, (2325):22–33.

Chenglong, L., Zhou, F., Jiafang, W., and Xiang, Z. (2015). A vortex-ring-state-avoiding descending control strategy for multi-rotor uavs. In *Chinese Control Conference (CCC), 2015 34th*, pages 4465–4471. IEEE.

Chi, Q. C., Bole, B., Hogge, E., Vazquez, S., Daigle, M., Celaya, J., and Weber, A. (2013). Battery charge depletion prediction on an electric aircraft.

CityAirbus (2017). https://www.airbus.com/newsroom/press-releases/en/2017/10/cityairbus-demonstrator-passes-major-propulsion-testing-mileston.html. [Online; accessed 18-January-2019].

Clarke, J.-P. B., Ho, N. T., Ren, L., Brown, J. A., Elmer, K. R., Tong, K.-O., and Wat, J. K. (2004). Continuous descent approach: Design and flight test for louisville international airport. *Journal of Aircraft*, 41(5):1054–1066.

Consulting, P. (2018). The future of vertical mobility. https://fedotov.co/wp-content/uploads/2018/03/Future-of-Vertical-Mobility.pdf. [Online; accessed 18-January-2019].

Coppenbarger, R., Lanier, R., Sweet, D., and Dorsky, S. (2004). Design and development of the en route descent advisor (eda) for conflict-free arrival metering. In *AIAA Guidance, Navigation, and Control Conference and Exhibit*, page 4875.

Coppenbarger, R. A., Mead, R. W., and Sweet, D. N. (2009). Field evaluation of the tailored arrivals concept for datalink-enabled continuous descent approach. *Journal of Aircraft*, 46(4):1200.

Dalmau, R., Verhoeven, R., de Gelder, N., and Prats, X. (2016). Performance comparison between temo and a typical fms in presence of cta and wind uncertainties. In *2016 IEEE/AIAA 35th Digital Avionics Systems Conference (DASC)*, pages 1–8.

Dear, R. G. (1976). The dynamic scheduling of aircraft in the near terminal area. Technical report, Cambridge, Mass.: Flight Transportation Laboratory, Massachusetts Institute .

DeMoss, J. A. (2007). *Drag measurements on an ellipsoidal body*. PhD thesis, Virginia Tech.

EHang-184 (2018). Ehang 184 autonomous aerial vehicle specs. http://www.ehang.com/ehang184/specs/. [Online; accessed 14-November-2018].

Erzberger, H. and Itoh, E. (2014). Design principles and algorithms for air traffic arrival scheduling.

Falck, R. D., Chin, J., Schnulo, S. L., Burt, J. M., and Gray, J. S. (2017). Trajectory optimization of electric aircraft subject to subsystem thermal constraints. In *18th AIAA/ISSMO Multidisciplinary Analysis and Optimization Conference*, page 4002.

Garg, D., Patterson, M., Hager, W. W., Rao, A. V., Benson, D. A., and Huntington, G. T. (2010). A unified framework for the numerical solution of optimal control problems using pseudospectral methods. *Automatica*, 46(11):1843–1851.

Gauntt, R. D. (2012). Aircraft course optimization tool using gpops matlab code. Technical report, Air Force Institute of Technology.

Goebel, K. and Saha, B. (2015). Prognostics applied to electric propulsion uav. In *Handbook of Unmanned Aerial Vehicles*, pages 1053–1070. Springer.

Hamilton, B. A. (2018). Urban air mobility (uam) market study. https://www.nasa.gov/sites/default/files/atoms/files/bah_uam_executive_briefing_181005_tagged.pdf. [Online; accessed 18-January-2019].

Heyson, H. H. (1975). A momentum analysis of helicopters and autogyros in inclined descent, with comments on operational restrictions.

Hoehner, C. M., Barlow, C. E., Allen, P., and Schootman, M. (2012). Commuting distance, cardiorespiratory fitness, and metabolic risk. *American journal of preventive medicine*, 42(6):571–578.

Hoffmann, G., Huang, H., Waslander, S., and Tomlin, C. (2007). Quadrotor helicopter flight dynamics and control: Theory and experiment. In *AIAA Guidance, Navigation and Control Conference and Exhibit*, page 6461.

Hong, Y., Lee, S., Lee, K., and Kim, Y. (2018). Optimal scheduling algorithm for air traffic point merge system using milp. In *Advances in Aerospace Guidance, Navigation and Control*, pages 407–420. Springer.

Hu, X.-B. and Chen, W.-H. (2005). Genetic algorithm based on receding horizon control for arrival sequencing and scheduling. *Engineering Applications of Artificial Intelligence*, 18(5):633–642.

Jin, L., Cao, Y., and Sun, D. (2013). Investigation of potential fuel savings due to continuous-descent approach. *Journal of Aircraft*, 50(3):807–816.

Johnson, W. (1977). Helicopter optimal descent and landing after power loss.

Johnson, W. (2012). *Helicopter theory*. Courier Corporation.

Ketema, Y. and Zhao, Y. J. (2010). Micro air vehicle trajectory planning in winds. *Journal of Aircraft*, 47(4):1460–1463.

Kim, H. D., Perry, A. T., and Ansell, P. J. (2018). A review of distributed electric propulsion concepts for air vehicle technology. In *2018 AIAA/IEEE Electric Aircraft Technologies Symposium (EATS)*, pages 1–21. IEEE.

Kirk, D. E. (2012). *Optimal control theory: an introduction*. Courier Corporation.

Kleinbekman, I. C., Mitici, M. A., and Wei, P. (2018). evtol arrival sequencing and scheduling for on-demand urban air mobility. In *2018 IEEE/AIAA 37th Digital Avionics Systems Conference (DASC)*, pages 1–7. IEEE.

Klesh, A. T. and Kabamba, P. T. (2009). Solar-powered aircraft: Energy-optimal path planning and perpetual endurance. *Journal of guidance, control, and dynamics*, 32(4):1320–1329.

Kulkarni, C. S., Roychoudhury, I., and Schumann, J. (2018). On-board battery monitoring and prognostics for electric-propulsion aircraft. In *2018 AIAA/IEEE Electric Aircraft Technologies Symposium*, page 5034.

Leishman, J. (2002). *Principles of helicopter aerodynamics*. Cambridge Aerospace Series. Cambridge University Press.

Malik, W. and Jung, Y. C. (2016). Exact and heuristic algorithms for runway scheduling. In *16th AIAA Aviation Technology, Integration, and Operations Conference*, page 4072.

Meindl, B. and Templ, M. Analysis of commercial and free and open source solvers for the cell suppression problem.

Morbidi, F., Cano, R., and Lara, D. (2016). Minimum-energy path generation for a quadrotor uav. In *Robotics and Automation (ICRA), 2016 IEEE International Conference on*, pages 1492–1498. IEEE.

Mueller, E. R., Kopardekar, P. H., and Goodrich, K. H. (2017). Enabling airspace integration for high-density on-demand mobility operations. In *17th AIAA Aviation Technology, Integration, and Operations Conference*, page 3086.

Neuman, F. and Erzberger, H. (1990). Analysis of sequencing and scheduling methods for arrival traffic.

Neuman, F. and Erzberger, H. (1991). Analysis of delay reducing and fuel saving sequencing and spacing algorithms for arrival traffic.

Nikoleris, T., Chatterji, G. B., and Coppenbarger, R. A. (2016). Comparison of fuel consumption of descent trajectories under arrival metering. *Journal of Aircraft*, 53(6):1853–1864.

Park, S. G. and Clarke, J.-P. (2012). Vertical trajectory optimization for continuous descent arrival procedure. In *AIAA Guidance, Navigation, and Control Conference*, page 4757.

Pawelek, A., Dalmau Codina, R., Lichota, P., and Prats Menéndez, X. (2017). Arrival traffic synchronisation with required time of arrivals for fuel-efficient trajectories. In *Proceedings of the 17th ATIO-AIAA Aviation Technology, Integration, and Operations Conference*, pages 1–14.

Pradeep, P., Park, S. G., and Wei, P. (2018). Trajectory optimization of multirotor agricultural uavs. In *2018 IEEE Aerospace Conference*, pages 1–7.

Pradeep, P. and Wei, P. (2017). Predictability, variability and operational feasibility aspect of cda. In *Aerospace Conference, 2017 IEEE*, pages 1–14. IEEE.

Pradeep, P. and Wei, P. (2018a). Energy efficient arrival with rta constraint for urban evtol operations. In *2018 AIAA Aerospace Sciences Meeting*, page 2008.

Pradeep, P. and Wei, P. (2018b). Energy optimal speed profile for arrival of tandem tilt-wing evtol aircraft with rta constraint. In *Accepted by 2018 IEEE CSAA Guidance, Navigation and Control Conference*, pages 1–6.

Pradeep, P. and Wei, P. (2018c). Heuristic approach for arrival sequencing and scheduling for evtol aircraft in on-demand urban air mobility. In *Digital Avionics Systems Conference, 2018 IEEE/AIAA*. IEEE/AIAA.

Prevot, T., Lee, P., Callantine, T., Smith, N., and Palmer, E. (2003). Trajectory-oriented time-based arrival operations: Results and recommendations. In *ATM2003, FAA/Eurocontrol R&D Seminar, Budapest, Hungary*. Citeseer.

Prevot, T., Rios, J., Kopardekar, P., Robinson III, J. E., Johnson, M., and Jung, J. (2016). Uas traffic management (utm) concept of operations to safely enable low altitude flight operations. In *16th AIAA Aviation Technology, Integration, and Operations Conference*, page 3292.

Psaraftis, H. N. (1980). A dynamic programming approach for sequencing groups of identical jobs. *Operations Research*, 28(6):1347–1359.

Rao, A. V., Benson, D. A., Darby, C., Patterson, M. A., Francolin, C., Sanders, I., and Huntington, G. T. (2010). Algorithm 902: Gpops, a matlab software for solving multiple-phase optimal control problems using the gauss pseudospectral method. *ACM Transactions on Mathematical Software (TOMS)*, 37(2):22.

Reid, J. S. (2018). https://homepages.abdn.ac.uk/nph120/meteo/DroneFlight.pdf. [Online; accessed 18-March-2019].

Rivas, D., Valenzuela, A., and de Augusto, J. L. (2013). Computation of global trajectories of commercial transport aircraft. *Proceedings of the Institution of Mechanical Engineers, Part G: Journal of Aerospace Engineering*, 227(1):142–158.

Robinson III, J. and Kamgarpour, M. (2010). Benefits of continuous descent operations in high-density terminal airspace considering scheduling constraints. In *10th AIAA aviation technology, integration, and operations (ATIO) conference*, page 9115.

Schrank, D., Eisele, B., Lomax, T., and Bak, J. (2015). 2015 urban mobility scorecard. https://static.tti.tamu.edu/tti.tamu.edu/documents/mobility-scorecard-2015.pdf. [Online; accessed 18-January-2019].

Smedt, D. d., Bronsvoort, J., and McDonald, G. (2013). Controlled time of arrival feasibility analysis. http://icrat.org/seminarContent/seminar10/papers/242-De%20Smedt_0126131150-Final-Paper-4-17-13.pdf. [Online; accessed 18-January-2019].

Snyder, C. A. (2017). Personal rotorcraft design and performance with electric hybridization. https://ntrs.nasa.gov/archive/nasa/casi.ntrs.nasa.gov/20170005655.pdf. [Online; accessed 18-January-2019].

Stell, L. (2011). Prediction of top of descent location for idle-thrust descents. ATM.

Thipphavong, D. P., Apaza, R., Barmore, B., Battiste, V., Burian, B., Dao, Q., Feary, M., Go, S., Goodrich, Kenneth H, H. J., Idris, H. R., Kopardekar, P. H., Lachter, J. B., Neogi, N. A., Ng, H. K., Oseguera-Lohr, R. M., Patterson, M. D., and Verma, S. A. (2018). Urban air mobility airspace integration concepts and considerations. In *2018 Aviation Technology, Integration, and Operations Conference*, page 3676.

Tsuchiya, T., Ishii, H., Uchida, J., Ikaida, H., Gomi, H., Matayoshi, N., and Okuno, Y. (2009). Flight trajectory optimization to minimize ground noise in helicopter landing approach. *Journal of guidance, control, and dynamics*, 32(2):605–615.

Uber-Elevate (2016). Fast-forwarding to the future of on-demand, urban air transportation. https://www.uber.com/elevate.pdf. [Online; accessed 18-January-2019].

van Rossum, G. and de Boer, J. Interactively testing remote servers using the python programming language.

Vascik, P. D. and Hansman, R. J. (2019). Development of vertiport capacity envelopes and analysis of their sensitivity to topological and operational factors. In *AIAA Scitech 2019 Forum*, page 0526.

Volocopter (2018). https://www.volocopter.com/en/urban-mobility/. [Online; accessed 18-January-2019].

Wächter, A. and Biegler, L. T. (2006). On the implementation of an interior-point filter line-search algorithm for large-scale nonlinear programming. *Mathematical programming*, 106(1):25–57.

Willemain, T. R., Fan, H., and Ma, H. (2004). Statistical analysis of intervals between projected airport arrivals. *Rensselaer Polytechnic Inst., DSES Tech. Rept*, pages 38–04.

Wing, D. (2005). A potentially useful role for airborne separation in 4d-trajectory atm operations. In *AIAA 5th ATIO and16th Lighter-Than-Air Sys Tech. and Balloon Systems Conferences*, page 7336.

Xu, Y. and Prats, X. (2017). Including linear holding in air traffic flow management for flexible delay handling. *Journal of Air Transportation*, pages 123–137.

Yomchinda, T., Horn, J., and Langelaan, J. (2011). Flight path planning for descent-phase helicopter autorotation. In *AIAA Guidance, Navigation, and Control Conference*, page 6601.

Zhan, Z.-H., Zhang, J., Li, Y., Liu, O., Kwok, S., Ip, W., and Kaynak, O. (2010). An efficient ant colony system based on receding horizon control for the aircraft arrival sequencing and scheduling problem. *IEEE Transactions on Intelligent Transportation Systems*, 11(2):399–412.

APPENDIX. LATERAL TRAJECTORY OPTIMIZATION OF MULTIROTOR UAVs

Optimal Control Problem Formulation under Wind Conditions for Multirotor UAVs

Wind conditions significantly impact the multirotor UAVs because of their lightweight. Hence to fly a multirotor UAV on the planned flight plan with lateral and vertical deviations within set tolerances, the power consumption must be dynamically adjusted in real time to counteract the wind. Therefore, for the safety of the surrounding environment and success of the flight mission, it is critical to i) continuously monitor the battery capacity (state-of-charge (SOC) and remaining useful life (RUL)) of Li-Po batteries throughout the flight mission and ii) diagnose failures in electric propulsion system immediately [Bole et al. (2014); Kulkarni et al. (2018); Chi et al. (2013); Goebel and Saha (2015)]. However, battery capacity cannot be measured directly and depends, in a highly non-linear way, on numerous factors such as the age of the battery, number of loading cycles, temperature, and drawn current [Kulkarni et al. (2018)]. Therefore, Battery Health Management (BHM) research is focused on creation of prognostic algorithms that can provide accurate estimates of battery storage capacity during flight planning and accurate indication of remaining charge during flight [Bole et al. (2014); Kulkarni et al. (2018); Chi et al. (2013)]. The optimal control problem formulation is performed by assuming point mass model of the multirotor UAV with quasi-steady flight, in a fixed inertial frame of reference (local North East Down (NED)) as shown in Figure [.1].

Flight Dynamics Modeling

In general, multirotor UAVs (quadcopters, hexacopters and octocopters) have more symmetrical i) fuselage shape and ii) location and orientation of rotors with respect to the center of mass than

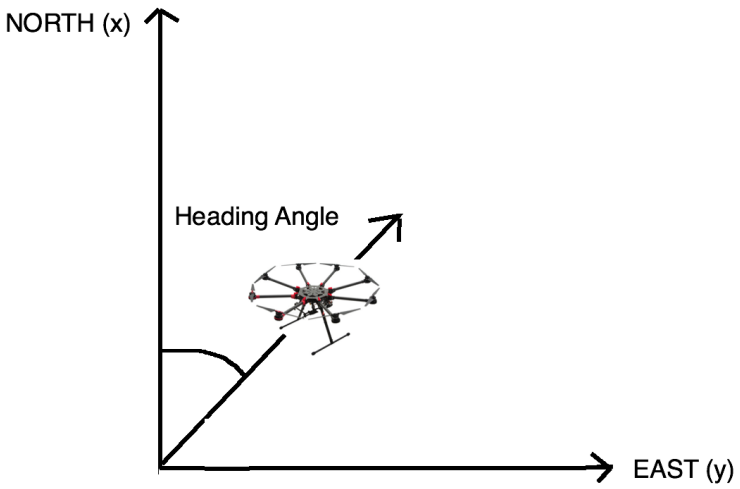

Figure .1: Local NED Frame of Reference

helicopters [Pradeep et al. (2018); Pradeep and Wei (2018a)]. Hence, longitudinal and lateral dynamics of multirotor UAVs can be decoupled from one another, given that it has already been done for helicopters by a few researchers [Bottasso et al. (2005); Yomchinda et al. (2011); Johnson (2012); Heyson (1975)].

Cruise Flight Dynamics

As stated earlier, the flight mission is assumed to be consisting of cruise phase at a constant altitude and heading angle. However, to study the affect of wind on cruise phase it is essential to extend the model to two spatial dimensions with the added lateral states (x, y, ψ), where ψ is the heading angle [Yomchinda et al. (2011); Tsuchiya et al. (2009)]. The multirotor UAV is assumed to have zero slide slip. The three control variables are: the net thrust (T), the rotor tip path plane pitch angle (θ) and the roll (bank) angle (ϕ). Therefore, the quasi-steady cruise flight dynamics of a multirotor UAV under wind conditions in a vehicle carried frame of reference are as follows [Pradeep et al. (2018); Pradeep and Wei (2018a); Yomchinda et al. (2011); Tsuchiya et al. (2009); Park and Clarke (2012); Ketema and Zhao (2010)]:

$$\frac{dV_T}{dt} = \frac{T\cos\phi\sin\theta - D}{m} - \frac{dW_x}{dt}\cos\psi - \frac{dW_y}{dt}\sin\psi \tag{.1}$$

$$V_T\frac{d\psi}{dt} = \frac{T\sin\phi}{m} + \frac{dW_x}{dt}\sin\psi - \frac{dW_y}{dt}\cos\psi \tag{.2}$$

$$\frac{dx}{dt} = V_T\cos\psi + W_x \tag{.3}$$

$$\frac{dy}{dt} = V_T\sin\psi + W_y \tag{.4}$$

where D is the parasite drag, V_T is the true airspeed (assumed to have only horizontal component during the cruise), W_x and W_y are wind speeds in x and y directions.

For level flight with zero vertical wind:

$$T\cos\phi\cos\theta = mg \tag{.5}$$

where m is the mass of the UAV and g is the acceleration due to the gravity.

$$T = \sum_{i=1}^{N} T_i \tag{.6}$$

where T_i is the thrust produced by the i^{th} rotor, N is the total number of rotors and T is the net thrust.

The state vector of the problem is defined as follows:

$$[x, y, V_T, \psi]^T \tag{.7}$$

The control vector of the problem is defined as follows:

$$u(t) = [\theta, \phi, T]^T \tag{.8}$$

Drag Model

Based on the maximum ground speed of the vehicle (72 km/hr), the vehicle operates in M $<$ 0.3 flow regime and hence the drag force on the fuselage of the eVTOL air taxi can be modeled based on the incompressible flow theory. The net drag on the vehicle is assumed to be equivalent

to the drag on the fuselage of the vehicle. Therefore, the net drag on the vehicle is calculated as follows [Yomchinda et al. (2011); DeMoss (2007)]:

$$D = \frac{\rho V^2 C_D F}{2} \tag{.9}$$

where F is the equivalent flat plate area of the fuselage and $C_D = 1$ [Yomchinda et al. (2011)]. The horizontal and vertical components of the drag in fixed inertial frame of reference are as follows:

$$D_x = \frac{\rho V_x^2 C_D F_x}{2} \tag{.10}$$

$$D_h = \frac{\rho V_h^2 C_D F_h}{2} \tag{.11}$$

where F_x and F_h are the equivalent front and top flat plate area of the fuselage respectively.